QEX

May/June 2020

www.arrl.org

A Forum for Communications Experimenters

Issue No. 320

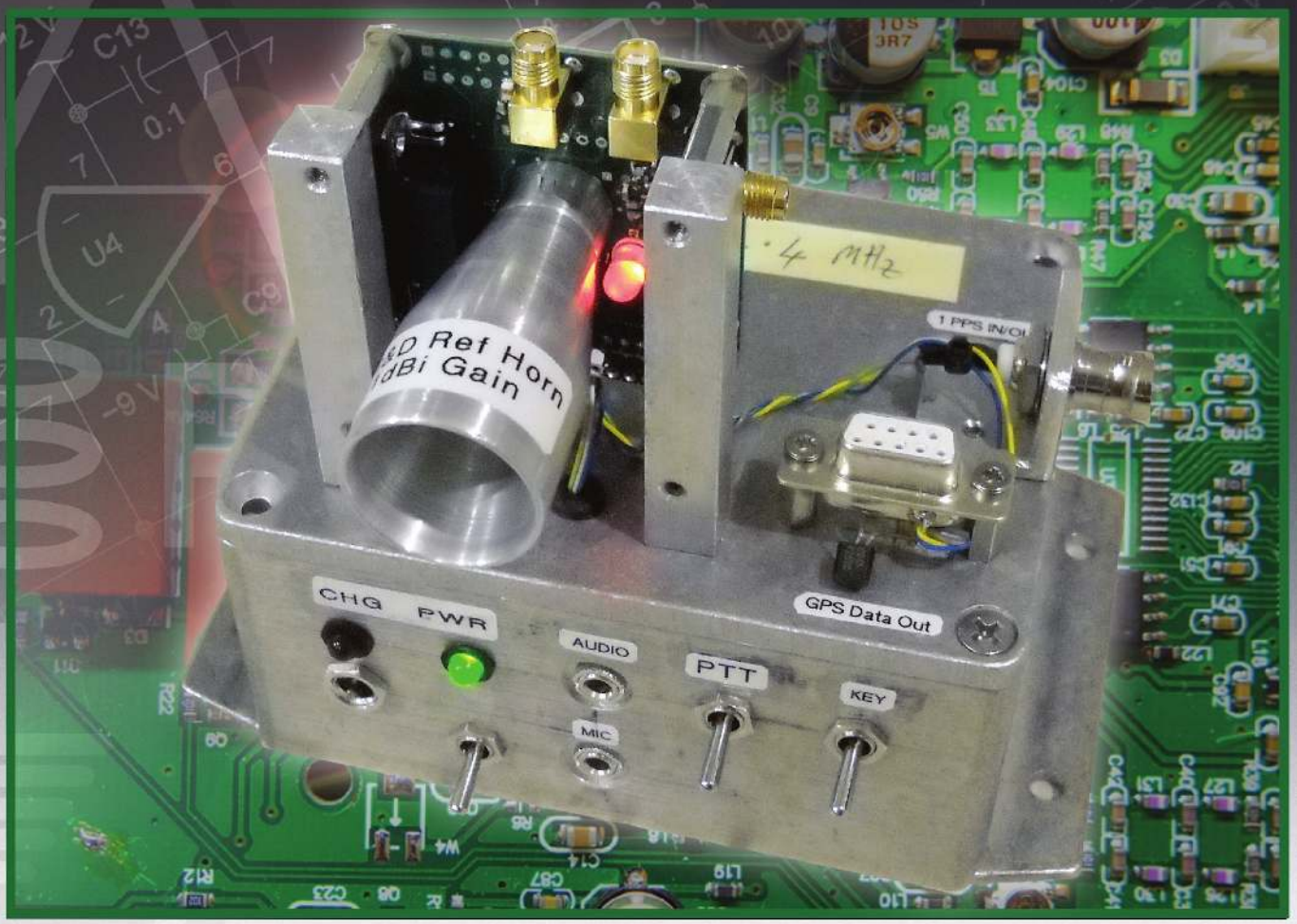

VK3CV/WQ1S designs a 122 GHz Transverter.

KENWOOD

3rd IMDR 110 dB*

RMDR 122 dB*

BDR 150 dB*

Performance Exceeding Expectations.

The most happy and sublime encounters happen in the worst circumstances and under the harshest conditions.

There are enthusiasts who know this all too well because of their love of HF radio.

Results born of certainty and not circumstance. Delivered through impeccable performance. This is our offering to you.

"The Kenwood TS-890S has the highest RMDR of any radio I have ever measured."

- Rob Sherwood - NC0B - December 2018

HF/50MHz TRANSCEIVER

TS-890S

NEW

Top-class receiving performance

3 kinds of dynamic range make for top-class performance.

- Third order intermodulation Dynamic Range (3rd IMDR) 110dB*
- Reciprocal Mixing Dynamic Range (RMDR) 122dB*
- Blocking Dynamic Range (BDR) 150dB*

*Values are measured examples. (2kHz spacing:14.1 MHz, CW, BW 500 Hz, Pre Amp OFF)

- Full Down Conversion RX
- High Carrier to Noise Ratio 1st LO
- H-mode mixer

4 kinds of built-in roofing filters

500Hz / 2.7kHz / 6kHz / 15kHz (270Hz Option)

7 inch Color TFT Display

- Roofing frequency sampling band scope
- Band scope auto-scroll mode
- Multi-information display including filter scope

Clean and tough 100W output

Built-in high-speed automatic antenna tuner

32-bit floating-point DSP for RX / TX and Bandscope

Customer Support: (310) 639-4200

www.kenwood.com/usa

ISO9001 Registered
JVCKENWOOD Corporation

ADS#02119

QEX

QEX (ISSN: 0886-8093) is published bimonthly in January, March, May, July, September, and November by the American Radio Relay League, 225 Main St., Newington, CT 06111-1494. Periodicals postage paid at Hartford, CT and at additional mailing offices.

POSTMASTER: Send address changes to: QEX, 225 Main St., Newington, CT 06111-1494 Issue No. 320

Publisher
American Radio Relay League

Kazimierz "Kai" Siwiak, KE4PT
Editor

Lori Weinberg, KB1EIB
Assistant Editor

Scotty Cowling, WA2DFI
Ray Mack, W5IFS
Contributing Editors

Production Department

Steve Ford, WB8IMY
Publications Manager

Michelle Bloom, WB1ENT
Production Supervisor

David Pingree, N1NAS
Senior Technical Illustrator

Brian Washing
Technical Illustrator

Advertising Information Contact:

Janet L. Rocco, W1JLR
Business Services
860-594-0203 – Direct
800-243-7768 – ARRL
860-594-4285 – Fax

Circulation Department

Cathy Stepina, *QEX Circulation*

Offices

225 Main St., Newington, CT 06111-1494 USA
Telephone: 860-594-0200
Fax: 860-594-0259 (24 hour direct line)
e-mail: **qex@arrl.org**

Subscription rate for 6 issues:

In the US: $29;

US by First Class Mail: $40;

International and Canada by Airmail: $35

Members are asked to include their membership control number or a label from their *QST* when applying.

In order to ensure prompt delivery, we ask that you periodically check the address information on your mailing label. If you find any inaccuracies, please contact the Circulation Department immediately. Thank you for your assistance.

About the Cover

Andrew J. Anderson, VK3CV/WQ1S, shows a simple, low cost way to get on the 122 GHz amateur band using an off-the-shelf integrated transceiver chip from Silicon Radar. The chip was originally designed for proximity measurements and radar applications. It features 0.5 mW RF output power, and the receiver path includes a preamplifier with a respectable noise figure. Its voltage controlled oscillator (VCO) can easily be frequency locked to an external phase locked loop (PLL) that operates at 1900 MHz. All the 122 GHz signals are inside the chip. The design interfaces the on-chip transmit and receive antennas to external high gain antennas.

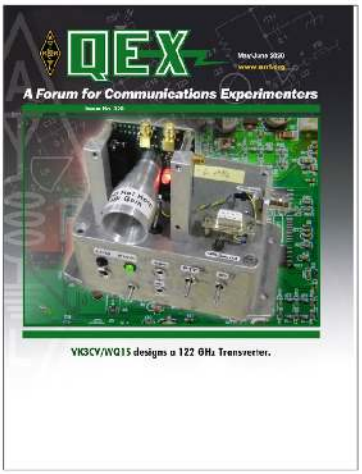

In This Issue

Features

Index of Advertisers

The American Radio Relay League

The American Radio Relay League, Inc, is a noncommercial association of radio amateurs, organized for the promotion of interest in Amateur Radio communication and experimentation, for the establishment of networks to provide communications in the event of disasters or other emergencies, for the advancement of the radio art and of the public welfare, for the representation of the radio amateur in legislative matters, and for the maintenance of fraternalism and a high standard of conduct.

ARRL is an incorporated association without capital stock chartered under the laws of the state of Connecticut, and is an exempt organization under Section 501(c)(3) of the Internal Revenue Code of 1986. Its affairs are governed by a Board of Directors, whose voting members are elected every three years by the general membership. The officers are elected or appointed by the Directors. The League is noncommercial, and no one who could gain financially from the shaping of its affairs is eligible for membership on its Board.

"Of, by, and for the radio amateur," ARRL numbers within its ranks the vast majority of active amateurs in the nation and has a proud history of achievement as the standard-bearer in amateur affairs.

A *bona fide* interest in Amateur Radio is the only essential qualification of membership; an Amateur Radio license is not a prerequisite, although full voting membership is granted only to licensed amateurs in the US.

Membership inquiries and general correspondence should be addressed to the administrative headquarters:

ARRL
225 Main St.
Newington, CT 06111 USA
Telephone: 860-594-0200
FAX: 860-594-0259 (24-hour direct line)

Officers

President: Rick Roderick, K5UR
P.O. Box 1463, Little Rock, AR 72203

The purpose of *QEX* is to:

1) provide a medium for the exchange of ideas and information among Amateur Radio experimenters,

2) document advanced technical work in the Amateur Radio field, and

3) support efforts to advance the state of the Amateur Radio art.

All correspondence concerning *QEX* should be addressed to the American Radio Relay League, 225 Main St., Newington, CT 06111 USA. Envelopes containing manuscripts and letters for publication in *QEX* should be marked Editor, *QEX*.

Both theoretical and practical technical articles are welcomed. Manuscripts should be submitted in word-processor format, if possible. We can redraw any figures as long as their content is clear. Photos should be glossy, color or black-and-white prints of at least the size they are to appear in *QEX* or high-resolution digital images (300 dots per inch or higher at the printed size). Further information for authors can be found on the Web at **www.arrl.org/qex/** or by e-mail to **qex@arrl.org**.

Any opinions expressed in *QEX* are those of the authors, not necessarily those of the Editor or the League. While we strive to ensure all material is technically correct, authors are expected to defend their own assertions. Products mentioned are included for your information only; no endorsement is implied. Readers are cautioned to verify the availability of products before sending money to vendors.

Kazimierz "Kai" Siwiak, KE4PT

Perspectives

QEX Joins the ARRL Online Offerings, Social DXing

QEX Online edition is now available as an ARRL member benefit. The printed edition of *QEX* is still be available to all subscribers including non-members at the usual subscription rates. *QEX* Online edition is the same as the printed magazine, but features full color. It joins the ARRL suite of digital magazines — *QST* Online, *On the Air*, and *NCJ* Online — that are all ARRL member benefits. In addition to the current issue, you will also find the January/February and March/April issues loaded onto the online platform.

For *QEX* authors that means a greatly expanded audience! For readers it represents access to the premier amateur radio technical journal for communications experimenters.

Amateur radio has been described as the original social media. We hams interact socially on a global scale with other hams from the comfort and the isolation of our arm chairs. We are sometimes rewarded by DXCC, WAS and other awards. Most importantly, we also use the medium for local as well as distant social and intellectual interaction. Social interaction takes on an added importance for our psychological well being. In today's reality isolation is a vital weapon in the fight against a dangerous global pandemic. Please check in with your ham friends by radio or by telephone or by whatever means is available to you. Keep up that connection during this time.

Let's make sure that an isolated friend, ham, or family member is not overlooked or forgotten. Stay in good health.

In This Issue

Jacek Pawlowski, SP3L, describes more new broadband wire antennas in this Part – 2.

Steve Stearns, K6OIK, explores general uniform transmission lines having complex characteristic impedance and propagation constant.

Bob DePierre, K8KI, extends the matching range of an 80 m antenna.

Andrew J. Anderson, VK3CV/WQ1S, gets on the 122 GHz band with a simple transverter.

Writing for *QEX*

Keep the full-length *QEX* articles flowing in, or share a **Technical Note** of several hundred words in length plus a figure or two. Let us know that your submission is intended as a **Note**. *QEX* is edited by Kazimierz "Kai" Siwiak, KE4PT, (**ksiwiak@arrl.org**) and is published bimonthly. The content is driven by you, the reader and prospective author. *QEX* is a forum for the free exchange of ideas among communications experimenters. All ARRL members can enjoy *QEX* Online edition as a member benefit. The printed edition annual subscription rate (6 issues per year) for members and non-members is $29 in the United States. First Class mail delivery in the US is available at an annual rate of $40. For international subscribers, including those in Canada and Mexico, *QEX* printed edition can be delivered by airmail for $35 annually, see **www.arrl.org/qex**.

Would you like to write for *QEX*? We pay $50 per published page for full articles and *QEX* Technical Notes. Get more information and an Author Guide at **www.arrl.org/qex-author-guide**. If you prefer postal mail, send a business-size self-addressed, stamped (US postage) envelope to: *QEX* Author Guide, c/o Maty Weinberg, ARRL, 225 Main St., Newington, CT 06111.

Very kindest regards,

Kazimierz "Kai" Siwiak, KE4PT

QEX Editor

Andrew J. Anderson, VK3CV/WQ1S

1 / 18 Glenmore Crescent, Black Rock, Victoria, 3193, Australia; **vk3cv_wq1s@yahoo.com**

A Simple 122 GHz Transverter

An easier way onto the 2.4 mm-wave band.

The 2.4 mm amateur band at 122.25 GHz to 123 GHz seems out of reach to many ham operators because the equipment can be very complex and requires a lot of experience to build. The very expensive components are hard to find and test equipment is rare.

That makes it a challenge! It is difficult to achieve long distance communications in the 2.4 mm band because of very high atmospheric absorption losses from oxygen and water vapor. To use the 122 GHz band we want cold still air at low pressure and low humidity. We don't want atmospheric pressure highs with thermal ducting and other high altitude atmospheric propagation enhancers. 122 GHz is more like visible light than RF. It's a winter band.

Much current 122 GHz equipment is based on high order frequency multipliers, which are low in efficiency and very low in output power. Receivers rarely have pre-amplification, so receive sensitivities are not good. Generating a detectable signal on 122 GHz is a considerable challenge.

This article presents a simpler, more compact and lower cost way to get operational on the band using an off-the-shelf, fully integrated transceiver chip originally designed for proximity measurement and radar applications. The chip technology is from Silicon Radar (**https://siliconradar.com/**). They design and manufacture a number of chips in the several gigahertz to more than 300 GHz range. For this project, a Silicon Radar chip is re-purposed as a narrow band transverter for ham radio use.

Pros and Cons of the Single Chip Approach

The Silicon Radar TRA_120 series chip contains a complete 118 to 126 GHz transceiver with separate integrated on-chip antennas for transmit and receive. The chip is available in two different packages with slightly different characteristics. **Figure 1** shows the chip block diagram. Data sheets are also available **[1]**.

The TRA_120 has some really nice features such as a relatively high power output of around 0.5 mW. At 122 GHz, half a milliwatt is high power. The chip receiver path includes a preamplifier with respectable gain and noise figure. It's also frequency agile since the internal oscillator is a Voltage Controlled Oscillator (VCO) that can easily be frequency locked using an external Phase Locked Loop (PLL).

The external PLL operates around 1900 MHz since the TRA_120 has a built in RF prescaler. There is no need to deal with 122 GHz signals on a PCB, all the 122 GHz signals are inside the chip.

There are some problems to solve first. Others who used the TRA_120 chip, notably Mike Lavelle, K6ML, quickly realized there's a major hurdle in that the on-chip transmit (TX) and receive (RX) antennas are not in the same exact physical place. This is fine if the chip is used bare as it was designed, or with a low gain external antenna. Because the chip TX and RX antennas are in different places, the TX and RX antenna patterns end up occurring at slightly different directions resulting in problems if a higher gain antenna is added. This means having to either re-position the chip or the antenna when swapping from TX to RX.

High gain antennas also introduce the challenge of getting them pointed at each other in the first place. Since the antenna gain is very high, the antenna beamwidth is very small. Pointing it exactly at the other station can be very challenging.

Because we have limited TX power and our RX is relatively deaf, high gain

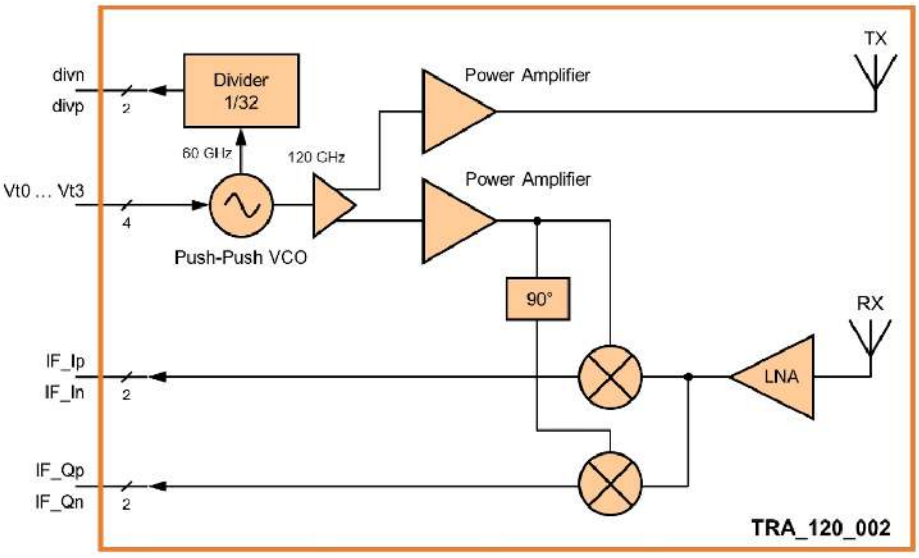

Figure 1 — The chip block diagram. [Source: siliconradar.com].

antennas are about the only easy way to add system gain to get any significant range performance. We must find a way to deal with the high gain antenna challenges.

We also need to deal with oscillator phase noise. Very careful PLL design, correct component selection, screening and noise source de-coupling are required to minimize phase noise. The PLL also multiplies the phase noise of the reference oscillator, so that needs to be the cleanest, lowest phase noise oscillator we can get: definitely a quartz crystal oscillator. The TRA_120 internal VCO adds phase noise as does the PLL chip and how it's configured. After many hours of development work it's all quiet enough to give a 3 - 4 quality tone in a narrow SSB receiver.

We need to be careful about frequency stability (drift). Since we'll need a PLL for the TRA_120 chip, we will also need a frequency reference, which could be a quartz crystal. Note that an error of 1 Hz in a 10 MHz reference translates to an error of over 12 kHz at 122 GHz. A GPS locked reference would help ensure the frequency error is low enough. I initially chose a lower cost (and lower dc power drain) voltage controlled, temperature compensated crystal oscillator (VCTCXO) to give me reasonably low phase noise. A voltage controlled oven controlled crystal oscillator (OCXO) would be even better but uses much more power and costs way more. If a good 10 MHz external reference is already available, use it. If an OCXO is used it's possible that GPS locking might not be required.

We can't generate SSB voice with this TRA_120 chip because we can't amplitude modulate the TX. However, we can easily generate angle modulations like FM or FSK. To generate pseudo Morse CW we switch the TX carrier on and off channel (FSK).

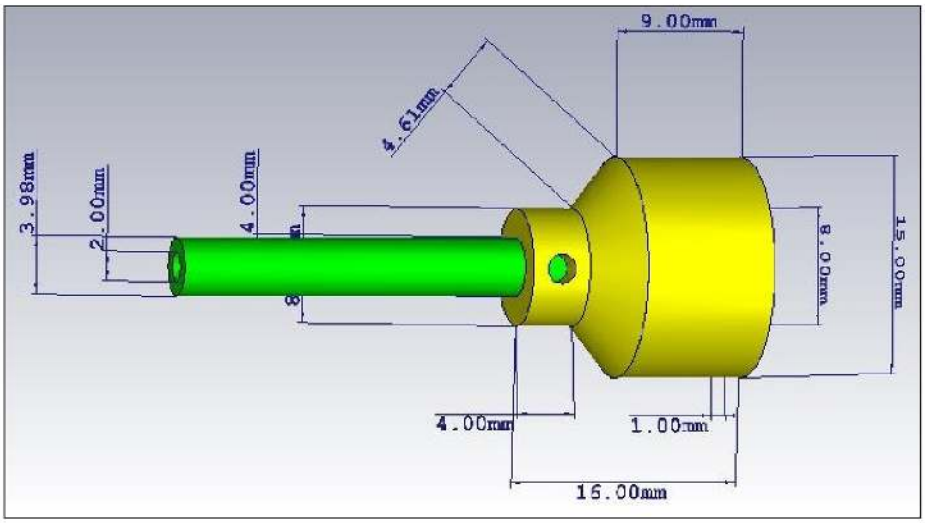

Figure 2 — The small diameter end is 2 mm circular waveguide. It is joined to the bell shaped coupler body that terminates in the chip on the rectangular PC board (not shown) attached to the large diameter end.

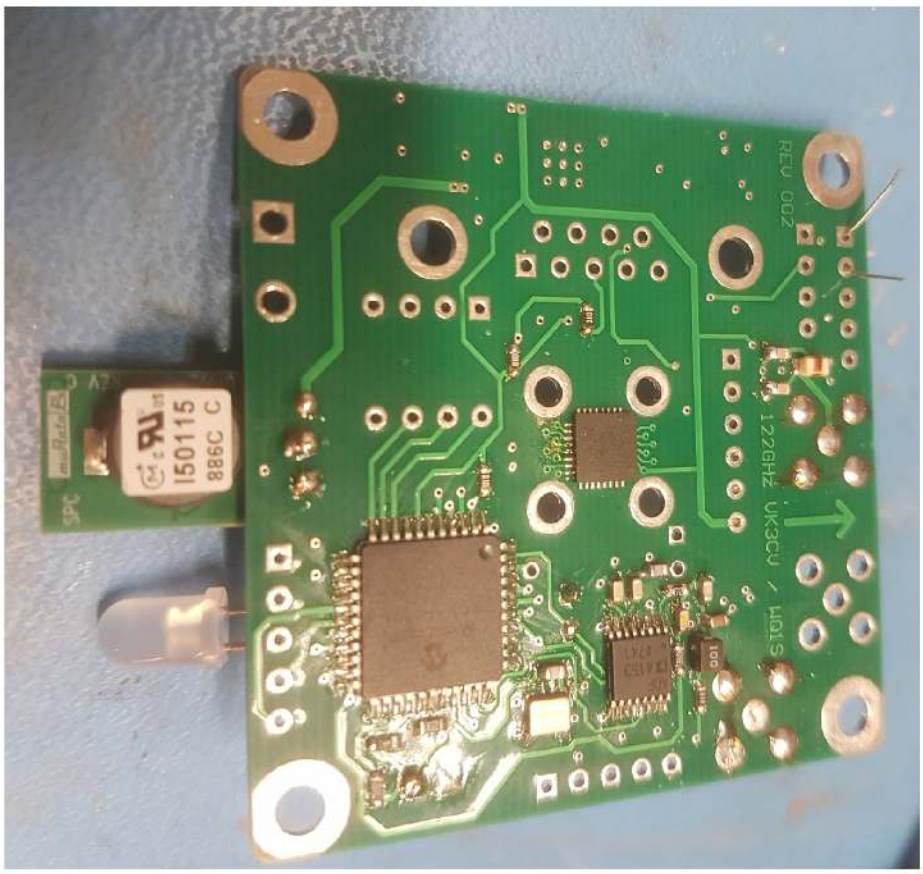

Figure 3 — PCB front side, note the TRA_120 chip in the center square hole pattern.

Problem Solving and Design Process

Let's first solve the antenna pointing problem. With a bit of lateral thinking and hours of simulation on the computer, I developed an RF chip coupler and combiner that you could call a duplexer (Figure 2). This coupler combines the RF from the on chip TX and RX antennas into a single waveguide path without the need for re-positioning the antenna from RX to TX. The downside is that we will lose some performance in both TX and RX. The TRA_120 comes in two versions, I chose the 002 version, which suits my coupler approach.

Mike Lavelle, K6ML, has very successfully used the 001 version with a servo driven feed re-positioner. Both approaches have their upsides and downsides. My coupler approach is simple to build. The re-positioning approach will give slightly better range performance because there are no coupler losses. It's up to you to decide. The coupler, **Figure 2**, is adjustable to allow optimization of the coupling and isolation.

No 122 GHz test equipment is needed, you can do it all with the S-meter and an attenuator on your IF receiver. The output of the coupler is a circular waveguide — it is in fact just a 5/64" (2 mm) diameter circular hole. The guide is circular but we are exciting it in a linear polarization.

Next, we need a high gain antenna to make this all work. Surplus satellite TV two-foot offset feed dishes are often to be found discarded in the trash. Many

microwave operators consider them junk. They actually work really nicely at 122 GHz if you take the time to set them up properly. The surface accuracy is generally very good, which is exactly what we need for 2.4 mm wavelengths. It really doesn't matter if the gain is a few dB down on what the theory says because of minor curvature errors. The price is right and a 2 ft reflector will produce over 50 dBi gain. One of these reflector antennas at each end gives us an overall system path gain boost of 100 dB. The transmit EIRP is 50 dB above 0.5 mW, or 50 W EIRP. You're going to hear that alright!

Let's Build It

Silicon Radar offers a development kit for the chips that others have used for experimentation. Since this project needs features outside the normal usage of the chip, a new PCB was designed just for the transverter. **Figure 3** shows the front side of the PCB with the TRA_120 chip in the center. This allows direct connection to a waveguide transition. **Figure 4** shows the back side of the PCB.

The PCB features an IF output with cable driver to an external receiver. It covers dc to 200 MHz and is I/Q output capable. The small PCB (2" × 2") allows mounting directly at the feed point of a dish. Low power consumption allows portable battery operation at 12 V dc, reverse polarity protected. The on-board PIC16LF877A microcontroller controls the TRA_120 and PLL. A 10 MHz GPS locked crystal frequency reference has extra outputs for other gear if required. A multi-channel switch is included for easy PLL channel frequency and mode change. Mode switching is included for FM voice, FM tone, pseudo-CW with a built in Morse beacon identifier. An RS-232 diagnostics output allows status monitoring and GPS data output to give you latitude and longitude.

Figure 5 shows a simplified system block diagram, and **Figure 6** shows the assembled PCB against the background of the original schematic. Full circuit schematics, PCB artwork, construction details, mechanical drawings and microprocessor code can be downloaded from **www.arrl.org/QEXfiles** (also **[2]**).

Circuit Theory of Operation

With reference to the simplified block diagram and circuit schematic, an external power supply of a nominal 12 V dc is applied through a reverse polarity protection diode to a 5 V regulator, then to a second 3.3 V regulator that supplies all the active circuits. All functional control for the board is handled by a PIC16LF877A microcontroller. The clock for the microcontroller and reference signal for the PLL is provided by a VCTCXO running at 10 MHz.

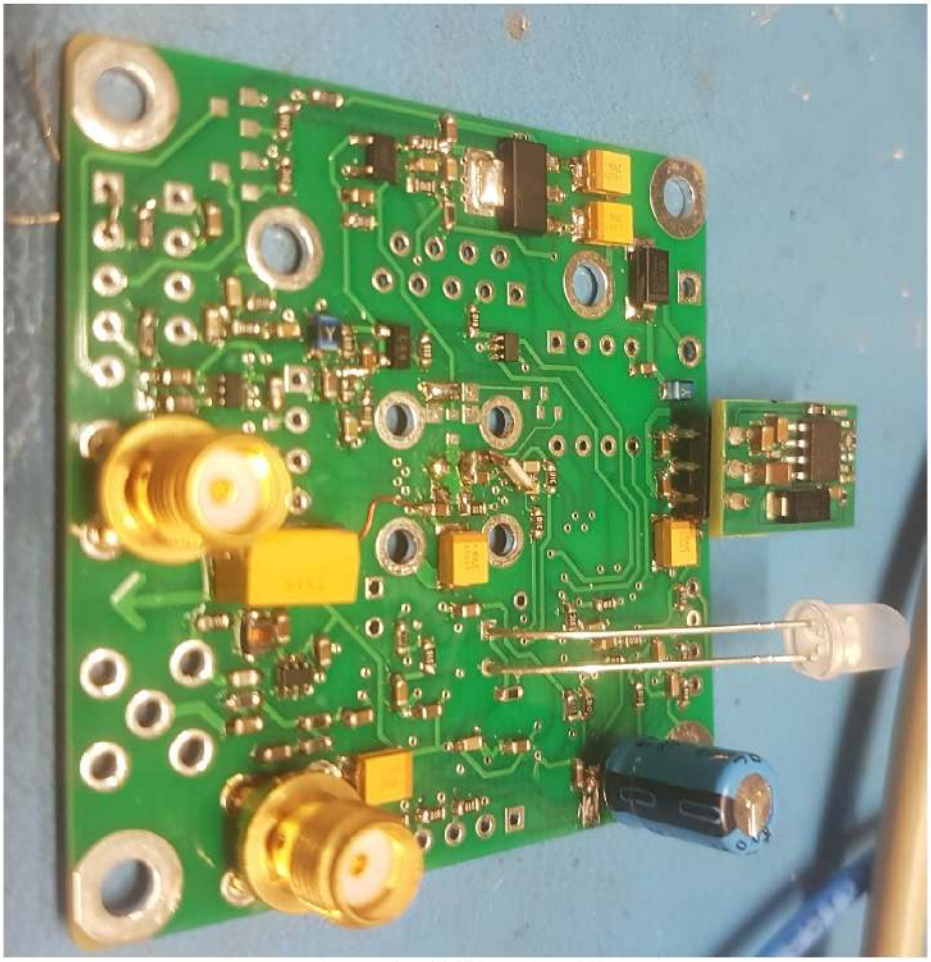

Figure 4 — PCB reverse side.

The 122 GHz transceiver chip is controlled by the microcontroller. The chip is frequency locked by the PLL (ADF4153). The 122 GHz TX and RX circuitry are all contained within the TRA_120_002 chip. A divide-by-64 output of the internal 122 GHz VCO in the TRA_120_002 chip is fed to the PLL, which can then lock its internal VCO to the desired operating frequency. The VCO in the TRA_120_002 is always operating either on the TX or RX frequency, and its frequency is determined by the control data sent to the PLL chip by the microcontroller.

The PLL operates in the region of 1.9 GHz. A test point is available to observe this 1.9 GHz signal to allow testing of the system. The PLL phase comparator output is fed via a loop filter to the VCO tune inputs of the TRA_120_002. This voltage is monitored by the microcontroller as well as by the PLL lock signal to ensure the PLL is correctly locked.

Modulation inputs are included in the PLL circuit to allow modulation of either the VCO error voltage or of the reference tune voltage, resulting in FM modulation of the VCO. There are selection links to choose which modulation path is used. Normally the reference signal path is used giving a nominal 5 kHz of FM deviation. The modulation signal is supplied from a simple modulation limiting microphone amplifier that is connected to an external electret type microphone.

The VCTCXO tune voltage is derived from a resistive voltage summing network. Inputs to this network are provided from the microcontroller to provide frequency error locking to an external GPS signal as well as FM tone modulation. An external GPS-derived one pulse per second (1 PPS) signal is fed to the microcontroller that, under software control, uses this to lock the 10 MHz internal reference to the external 1 PPS signal, resulting in a frequency error much

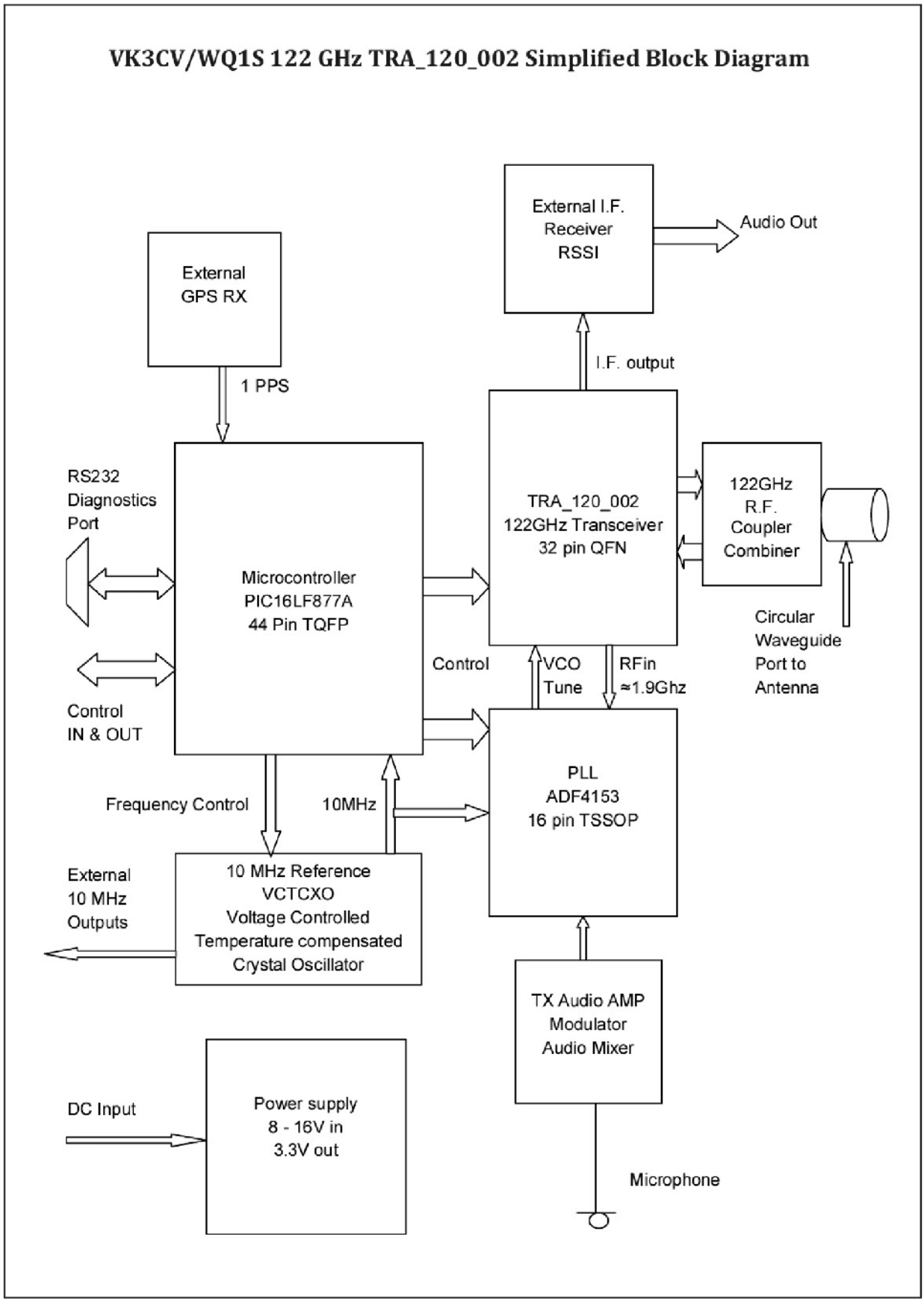

Figure 5 — System block diagram.

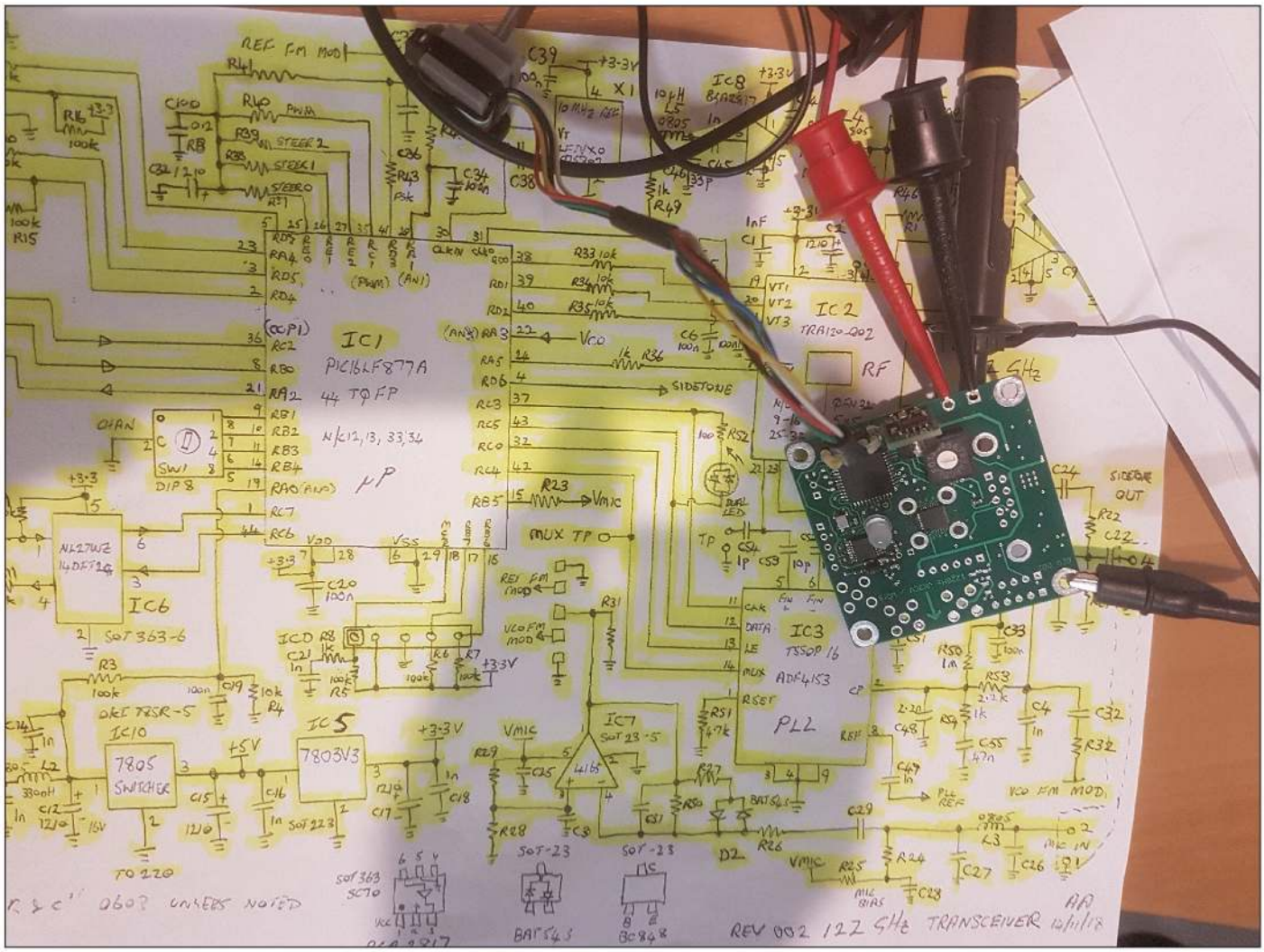

Figure 6 — Assembled PCB against the background of the original schematic.

less than 1 Hz when locked. The frequency-locked 10 MHz signal is also available externally and can be used as a reference for other equipment.

The TRA_120_002 chip has two separate internal linearly polarized antennas — one for TX and one for RX — that are separated physically within the structure of the chip. The TX and RX signals are combined in a specially designed external chip-to-waveguide coupler (Figure 2) that sits directly over the TRA_120_002. The coupler external antenna port is a 5/64" (2 mm) diameter circular waveguide that is then fed to an external antenna. This approach ensures that no errors in the antenna main lobe direction occur between TX and RX, which would be very significant if a high gain antenna were used without the coupler. The coupler feed waveguide is circular but the polarization remains linear. The marker arrow (top of Figure 3) on the PCB indicates the linear E-field polarization orientation. Two types of antennas were made, a Chaparral™ type with 10 dBi gain for use as an offset type dish feed, and a 21 dBi gain conical horn for beacon use. When the dish feed is used with a 2-ft dish, a gain of over 50 dBi is possible.

Received signals from the internal chip RX antenna on 122 GHz are first amplified and then converted down to the IF frequency by a mixer inside the TRA_120_002 chip. The IF signals are available as I/Q differential signals for use by an external software defined radio (SDR) or in an analog format via a buffer amplifier for use by an external IF receiver. The IF frequency is nominally 144.4 MHz. This can be changed to anywhere from dc to 200 MHz under software control. There is a significant amount of degradation in the FM received signal-to-noise performance of the system due to the inherent phase noise of the 122 GHz LO. Use of the narrowest IF bandwidth FM demodulator available will give the best results. Note that since the VCO in the TRA_120_002 is always running, full duplex operation is possible in FM mode. This is done by having the local system and the remote system operate on frequencies separated by the IF.

Transmit signals on 122 GHz originate from the VCO inside the TRA_120_002. They're then fed via an internal TX amplifier and then on to the internal chip TX antenna.

Software Operation

The microcontroller takes inputs from several sources, which it then uses to control various features and functions of the system under control of the internal software. The microcontroller has control of the following: bi-color red/green LED, FM modulation tone generation, external sidetone generation, GPS frequency locking, microphone amplifier enable, PLL RF frequency, RS-232 diagnostics

port, TRA_120_002 mode, external mode control inputs, external mode outputs and channel selection. Note that only 2 channels are currently used, with A and B corresponding to '0' and '1' on the least significant bit of the channel selection lines. If a channel switch is fitted to the PCB, the DIP switches must be set to all open or position '0' for a rotary HEX switch.

The system software is contained in flash memory within the microcontroller. Software programming is provided via the In-Circuit Serial Programming (ICSP) port on the board. Refer to the relevant microchip data sheets for information and software programming details.

On power up, the microcontroller configures all the required inputs and outputs and initializes the required internal registers and external peripherals. A dual-color LED gives operator feedback on operation. The LED initially glows red during power-on and then changes to green to show correct operation and that the PLL is locked. If the PLL is not locked, the LED will flash red. The LED will also glow red when the system is in the TX mode. A rapidly alternating red-green LED flash indicates low — less than approximately 10 V dc — input voltage.

Depending on the selected mode of operation, the microcontroller has a built-in Morse code keyer available that can provide a continually repeating Morse code message such as a call sign on the transmitter to aid with testing, and for use as a beacon. The transmitted string can be changed in the software as desired. It is located in the string definition section near the end of the assembly language file.

The full assembly language source code file is available on the **QEXfiles** web page and in the Dropbox archive [2]. All information in the archive is provided free of charge and without any direct or implied warranty.

Construction

The PCB is laid out to easily interface with the TRA_120 chip. The design is a 4 layer board with an almost continuous internal ground plane to keep all the signals where they're supposed to be. Mounting the chip is challenging. Good optical magnification, a steady hand and a source of heat are needed. There are plenty of YouTube videos on how to do it. It's suggested to mount the TRA_120 chip first. Observe basic anti-static practices, although the chip is quite robust in this respect. Once the chip is down, as a sanity check you can measure with an ohm meter at all the chip signal pins to ground to check if there is a diode junction present on all the connected pins. The diodes that you see with the meter are ESD protection on all the pins. Reflow the chip again if there are any issues. Everything else can be placed and soldered manually using a small tip iron with the assistance of optical magnification.

Any external GPS board that has a one pulse per second (1 PPS) output is suitable for the oscillator disciplining. I mounted the GPS receivers in a small external plastic box that plugs into the control box with a separate regulator to reduce noise.

Figure 7 — Tool used to bore out the internal tapered hole in the conical horns.

Figure 8 — Machining of the Chaparral feed uses a special tool made from a broken tap.

Firing Up the System

Now the fun stuff. First, get two boards with bare chips to communicate across the shack to see that the thing actually works. If you have some test gear it's also possible to see the 1.9 GHz PLL signals and check that everything is locked and stable. No test gear on 122 GHz is required. Diagnostics data is also available on the RS-232 port at 9600/8-N-1.

Several options for antennas are possible, including bare chips, conical horns made

on a lathe (**Figure 7** and **Figure 8**), and dishes. All the antennas, feeds and coupler mechanical details are in the **QEXfiles** web page and in the Dropbox archive [2]. The Chaparral feed is machined using a special tool made from a broken tap (Figure 8). Another tool (Figure 7) was made to bore out the internal tapered holes in the conical horns. **Figure 9** shows a horn antenna, and adjustable and fixed feeds, compared with a 25 mm diameter coin.

The ultimate step is to use the larger dishes. Good stable tripods and telescopic sights are required when you get to this point. A purpose-designed multi-choke ring feed (commonly known as a Chaparral feed) was made for the dishes. Experiments were done with both a fixed and adjustable coupler and feed. The adjustable one works much better and is documented in the archive. The adjustable version allows optimization of the chip coupler. The chip coupler/combiner is built into the PCB waveguide mounting flange. The dish feeds have about 9 dBi gain to suitably illuminate the dishes.

As a sanity check, a comparison was made between the Chaparral feed and the bare chip. The difference is around 1 dB, which suggests the feed is working very well indeed. The bare chip antenna gain is about 10 dBi according to the chip specifications.

Figure 10 shows the feed point and the telescopic sight. **Figure 11** shows the control box (bare metal) with GPS unit (black plastic) atop. **Figure 12** shows the assembled station ready for action.

Setting up the dishes is time consuming. You'll need to be patient and methodical. Set up one of the boards with a bare chip out past the RF near zone at 25 yards from the dish system. Try to have the test area clear of reflective objects, which at 122 GHz is just about anything. Connect your IF receiver to the test unit and put an adjustable attenuator in the line if you have one. The attenuator is handy to keep the S-meter on your receiver in a useful range. The IF is 144 MHz.

The optimum feed point of the dish must be correctly identified in all three dimensions X,Y and Z. A good starting point is the original position of the old satellite feed. Use trial and error by peaking for maximum signal from the remote beacon board. Accuracy and stability are important here. The feed positioning accuracy needs to be less than a 1/32" in each of X,Y and Z planes to realize peak gain. Also each time you move the feed, the dish needs to be re-peaked to see the effect. It took a few days to do both dishes. A temporary mounting bracket with slotted holes to hold the TRA_120 board in the dish focus point to allow everything to be adjusted is very useful. Make small changes then record the peak result and also the size and number of significant side lobes. Generally there are more and larger side lobes when the feed is not in the right place. It's just like focusing an optical lens. The image needs to be sharp, not fuzzy. Lots of side-lobes indicate bad focus. When correctly focused, the dish is by-design meant to have few and small side-lobes. A 2-ft dish should realize over 50 dBi of gain and have a 3 dB beamwidth of around 0.3°. Optical telescopic sights are very useful to achieve alignment once the feeds are set up correctly. Align the optical

Figure 9 — A horn antenna, and adjustable and fixed feeds.

Figure 10 — The feed point and the telescopic sight.

Figure 11 — The control box (bare metal) with GPS unit (black) atop.

Figure 12 — The assembled station ready for action.

sights after the dish feed positions are optimized in the field by using a far field test. You'll need a 600 yard dish-to-dish distance to align the sights correctly.

The dish itself (Figure 12) will end up at an angle normally around 20° to 30° in the vertical plane when the actual main lobe is perfectly horizontal. This is due to the offset feed arrangement. Not all satellite dishes are created equal however. Don't assume that just because you have two dishes that visually look similar, that they are exactly the same as far as the optimum feed position is concerned. Offset feed dishes give slightly better gain than prime focus dishes because there is less feed obstruction.

There are added adjustable stabilizing rods to the sides of the dish and back to the feed point. This helps keep everything stable, especially going up to a mountain top to try to make some contacts. The adjustment rods also assist in realizing a few more dB of gain by slightly changing the shape of the dishes to be closer to the ideal shape. Again, careful adjustment and trial and error will get peak efficiency and thus peak gain.

The final systems are housed in a box with the control switches, a rechargeable battery, attached telescopic optical sights, and a bubble level to get the system perfectly horizontal to aid pointing in the right direction (Figure 11). Note that the arrow on the PCB (Figure 3) shows the polarization sense.

Three systems have been built so far, two dish systems (Figure 12) and a development system (**Figure 13**) that is useful as a test beacon and also as a mobile station. The inside of the feed box is shown in **Figure 14**.

Does It Actually Work?

The results in the field are impressive. First contacts had large margin, and were

Figure 13 — A development unit.

from dish to horn at more than 3 miles at sea level (**Figure 15**). A mobile contact was made at over 1.8 miles distance. The next step was 12 miles dish-to-dish in good atmospheric conditions at an altitude of 1000 feet, with more than 30 dB of margin. More mountain sites are yet to be conquered but currently the performance has been pushed out to over 36 miles. The system is expected to push the range out to something above 50 miles in ideal conditions. Definitely more distance is possible with very tall mountains but there aren't any of these in Australia. A mountain on a calm day in winter like Mt. Washington in New Hampshire would be ideal.

The system as described is programmed to be full duplex. That is, each end is offset in frequency by the IF. A headset with an attached boom microphone is ideal to chat away. Really interesting propagation effects can be observed due to air movement QSB, Doppler chirps from passing cars, and just dealing with the extra losses due to water vapor and air pressure. These are some of the charms of 122 GHz. The system as described supports NBFM and CW. Residual phase noise will be evident on FM.

Future work includes using the I/Q outputs of the TRA_120 to go directly to a Software Defined Radio IF and demodulator. TX with digital modes such as WSJT-X is also a possibility. There's a lot of experimenting and further development to be done, including a version of the PCB that uses a newer TRA_120_031 chip from Silicon Radar capable of operating at the next band up at 134 to 141 GHz.

Suggestions and comments are welcomed. QSY to 2.4 mm!

Acknowledgments.

I thank Silicon Radar for making the "magic" chips that made all this possible, and for their excellent support. Thanks to Sally, my spouse, for helping with field measurements and for keeping me watered and fed. Thanks to Ken Anderson, my late Dad, he taught me how to use my brain, my hands, and a lathe; and also to the late Les Jenkins, VK3ZBJ, — my mate and mentor — "what Uncle Les didn't know about RF isn't worth knowing." Thanks go to Karl Harbeck, VK3LN, for field operations, assistance and sourcing the surplus dishes; and to Noel Higgins, VK3NH, for field operations and assistance; to Mike Lavelle, K6ML; Alan Devlin, VK3XPD; Dave Smith, VK3HZ; and others for ideas and peer review.

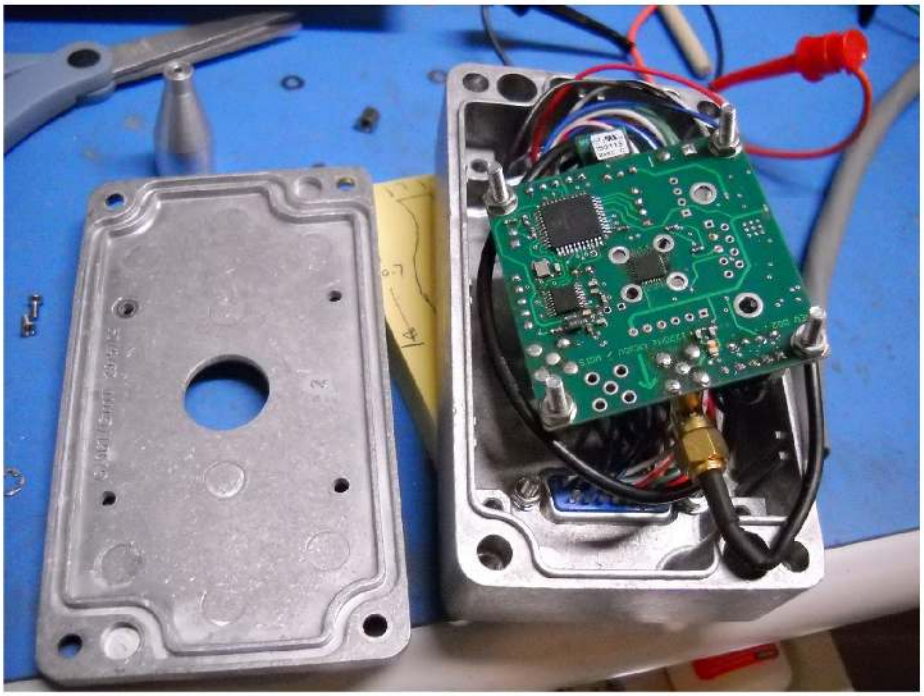

Figure 14 — Inside the dish feed box.

[Photos by the author].

Andrew Anderson, VK3CV / WQ1S was first licensed in 1976 as a Novice in Australia (VK3NQU) at age 15. His first contacts were on 80 m with an army surplus Second World War AM / CW British C11 tank transmitter and a borrowed Trio 9R59D receiver. He built his first 2 m station while still in high school. He also constructed a 50 ft tilt-over tower, a shack below the tower, a transverter to a 10 m IF, and a 200 W 4CX250 power amplifier. Andrew studied electronics at RMIT in Melbourne, Australia from 1979 to 1983. He soon achieved a limited Technical Class license, VK3YPD. He gradually became more interested in VHF, UHF and SHF bands using a mix of modified commercial and home brew equipment. In 1980 he consolidated his Novice and Limited call, later becoming VK3CV. Andrew has held many distance records in Australia from 144 MHz up to 122 GHz.

Andrew lived and worked near Boston MA, USA, and in 2009 obtained his US Amateur Extra class license AB1LA, later changed to WQ1S. He is now semi-retired and spends more time in Australia. He enjoys experimenting on the millimeter and sub-millimeter bands, and machining his own mechanical hardware.

Figure 15 — VK3CV, operating from the Cerberus Car Park, Black Rock, Victoria, Australia.

Notes

[1] See **https://siliconradar.com/datasheets/Datasheet_TRA_120_002_V0.8.pdf**.

[2] See **https://www.dropbox.com/sh/oesw3j4jwrf1pb2/AAA06dkaindVJy8k0dbw82B9a?dl=0**.

Steve Stearns, K6OIK

P.O. Box 4917, Mountain View, CA 94040-0917; **k6oik@arrl.net**

General Uniform Transmission Lines: Power Efficiency, Loss, Standing Wave Ratio, and Return Loss

An exploration of general uniform transmission line having complex characteristic impedance and propagation constant.

This tutorial article explores general uniform transmission line that has complex characteristic impedance and propagation constant. Apparent and real paradoxes involving terminated lines are given. Correct general formulas for power efficiency, loss, standing wave ratio, and the return loss of complex-terminated general uniform transmission lines are developed. Pseudo-waves such as power waves and 'new' power waves are described. Various 'return loss' definitions are reviewed and compared. A bibliography lists the major classical treatments of transmission line theory.

Introduction

This work explores the general uniform line that has complex characteristic impedance and propagation constant. We begin with three paradoxes of transmission line theory that motivated the present work. In the process of explaining these paradoxes, we introduce correct general formulas for power efficiency, loss, standing wave ratio, and the return loss of complex-terminated general uniform transmission line. We describe traveling waves and pseudo-waves such as power waves and 'new' power waves that are useful for complex port impedance in multiport networks. A variety of different definitions of return loss are reviewed and compared via numerical examples. The paper concludes with a fourth paradox that is little known, deeper, and not easily resolved. The issues addressed have counterparts in electromagnetic field theory, particularly wave mechanics in linear media and reflections at interfaces of complex materials including metamaterials, as well as in the theory of non-Foster artificial lines. These connections are mentioned. Several elementary identities of complex-valued hyperbolic trigonometric functions of a complex variable are necessary to understand the past and present work. Basic facts about hyperbolic trigonometric functions, including identities, series, integrals, products, and inequalities, can be found in standard handbooks, e.g. **[1]**, **[2]**, **[3]**. The major classical treatments of transmission line theory were examined, starting from Heaviside. Of these older works, few addressed transmission line analysis with the generality of the present work. None anticipated all the paradoxes.

Paradox 1: Reflection Coefficient Magnitude Greater than Unity

Real transmission lines are lossy. At a frequency, if a line doesn't satisfy the Heaviside cross-ratio condition then the line's characteristic impedance is a complex number, which we will denote as $Z_0 = R_0 + jX_0$. See the **Sidebar: Heaviside Transmission Line**. Suppose that a load impedance is a pure reactance equal to $-X_0$. Then,

$$\begin{aligned}\Gamma_L &= \frac{Z_L - Z_0}{Z_L + Z_0} \\ &= \frac{(R_L - R_0) + j(X_L - X_0)}{(R_L + R_0) + j(X_L + X_0)} \\ &= -\left(\frac{R_0 + j2X_0}{R_0}\right) \\ &= -\left(1 + j\frac{2X_0}{R_0}\right)\end{aligned} \tag{1}$$

The magnitude of the reflection coefficient is then

$$|\Gamma_L| = \sqrt{1 + 4\left(\frac{X_0}{R_0}\right)^2} > 1 \tag{2}$$

which exceeds unity.

This paradox is a surprising but true result. It is not the result of an error caused by using formulas incorrectly. It can be shown that the magnitude of the reflection coefficient can be as great as, but no greater than $1+\sqrt{2}=2.414...$. The phase angle of a characteristic impedance is restricted to the quadrant $\pm\pi/4$ radians ($\pm 45°$), cf. **[4, pp. 136-137]**. Setting $X_0 = R_0$ in (2) gives $|\Gamma_L| = \sqrt{5} = 2.236$, which is close to the maximum value.

Paradox 2: Negative SWR

If the magnitude of a reflection coefficient exceeds unity, $|\Gamma_L| > 1$, then a common formula for SWR gives

$$\text{SWR} = \frac{1+|\Gamma_L|}{1-|\Gamma_L|} < -1 \tag{3}$$

We might erroneously conclude that negative SWR < -1 is possible when Z_0 is complex as assumed above. SWR between -1 and +1 is prohibited in any case. This paradox is the result of misapplying a formula that is valid for real Z_0 to a line for which Z_0 is complex. A general formula for SWR proved below always gives SWR ≥ 1.

Paradox 3: Sub-Unity Return Loss

The standard definition of return loss is the reciprocal of the squared magnitude of the reflection coefficient.

$$\text{Return Loss} = \frac{1}{|\Gamma_L|^2} \tag{4}$$

Ordinarily $|\Gamma_L| < 1$, and return loss is a number greater than unity, or positive in decibels. However if $|\Gamma_L| > 1$, as above, then return loss given by (4) is less than unity. In decibels, the return loss, then, is negative. This is paradoxical because it seems to mean the reverse power reflected from a passive load is greater than the forward power that is incident on the load. As in the case of negative SWR, this paradox is the result of misapplying a formula that is valid for real Z_0 to a line for which Z_0 is complex. However, unlike SWR, a unique formula cannot be easily given. The reasons are discussed below.

Analysis

These first three paradoxes all rely on Z_0 being complex. The paradoxes seem strange because so many of the facts and formulas we know about transmission lines are true only if Z_0 is real. We explore these matters in some detail below.

Given a terminated transmission line of length l, the transfer function or ratio of output to input complex phasor voltage and current are given in R.A. Chipman's book on transmission line theory **[4]** as

$$\frac{V_T}{V_i} = \frac{1}{\cosh\gamma l + \frac{Z_0}{Z_T}\sinh\gamma l}$$

$$\frac{I_T}{I_i} = \frac{1}{\cosh\gamma l + \frac{Z_T}{Z_0}\sinh\gamma l}$$

and in the ARRL Antenna Book **[5]** as

$$\frac{E_L}{E_{in}} = \cosh\gamma l - \frac{Z_0}{Z_{in}}\sinh\gamma l$$

$$\frac{I_L}{I_{in}} = \cosh\gamma l - \frac{Z_{in}}{Z_0}\sinh\gamma l$$

where subscripts "T" or "L" mean the terminated or load end, sinh(·) and cosh(·) are the complex-valued hyperbolic sine and hyperbolic cosine functions of a complex variable, and $\gamma = \alpha + j\beta$ is the complex propagation constant. Since these are phasor equations, they are valid at a given frequency. In other words, these are steady-state "frequency domain" equations that depend on frequency. The equations can be derived from the 2-port *ABCD* or chain matrix of a uniform transmission line section of length l.

$$\begin{bmatrix} E_{in} \\ I_{in} \end{bmatrix} = \begin{bmatrix} \cosh\gamma l & Z_0\sinh\gamma l \\ \frac{1}{Z_0}\sinh\gamma l & \cosh\gamma l \end{bmatrix} \begin{bmatrix} E_L \\ I_L \end{bmatrix} \tag{5}$$

As a matter of terminology, we avoid the term "transmission" or "T matrix" to avoid confusion with another 2-port transmission matrix that involves normalized wave quantities instead of voltages and currents **[6, pp. 605 and 609-612]**. Load quantities in (5) can be expressed in terms of the input quantities by matrix inversion.

$$\begin{bmatrix} E_L \\ I_L \end{bmatrix} = \begin{bmatrix} \cosh\gamma l & -Z_0\sinh\gamma l \\ -\frac{1}{Z_0}\sinh\gamma l & \cosh\gamma l \end{bmatrix} \begin{bmatrix} E_{in} \\ I_{in} \end{bmatrix} \tag{6}$$

Heaviside Transmission Line

Heaviside line is ideal uniform transmission line for which the distributed parameters *R*, *L*, *G*, and *C* are constant independent of both frequency and position and which satisfy the cross ratio condition.

$$\frac{R}{L} = \frac{G}{C} \quad \text{or} \quad RC = LG \quad \text{or} \quad \frac{R}{G} = \frac{L}{C}$$

Such line has important properties, the chief ones are:

(a) The line is dispersionless and, moreover, distortionless

(b) The characteristic impedance is a real constant

(c) Dissipation (heating) is monotone along the line because ohmic and dielectric losses are balanced. Neither dominates.

(d) The delivered power at a point (or reference plane) anywhere along the line equals the difference between the powers in the forward traveling wave and the reverse traveling wave at that point.

No practical transmission line satisfies these conditions. For most practical lines, series ohmic losses are much greater than shunt dielectric losses. Hence (a) – (d) are approximations at best. Certain types of RF wattmeters depend on (d) being true. For practical, lossy lines and high SWR loads the net delivered power calculated from measurements made by such wattmeters can be in error by many dB.

For a uniform transmission line, if *R*, *L*, *G*, or *C* vary with frequency, they might happen to satisfy the cross ratio condition at some frequency. In this case, (b) – (d) are true at the frequency, although (a) is not.

It is noted that the currents have the same direction in (6) as in (5). If the current directions are reversed, the 2nd row and 2nd column of (6) are negated, and one recovers (5) with the input and output ports reversed. Thus we have proved that a transmission line section is a symmetrical 2-port. It behaves the same if it is flipped end for end.

To obtain Chipman's voltage equation, we substitute the load constraint $I_L = E_L/Z_L$ into the equation given by the first row of (5), obtaining

$$E_{in} = \left(\cosh\gamma l + \frac{Z_0}{Z_L}\sinh\gamma l\right) E_L \quad \text{or} \quad \frac{E_L}{E_{in}} = \frac{1}{\cosh\gamma l + \frac{Z_0}{Z_L}\sinh\gamma l} \tag{7}$$

which is the same as Chipman's voltage equation apart from notation differences.

To obtain Chipman's current equation, we substitute the load constraint $E_L = I_L Z_L$ into the equation given by the second row of (5), which yields

$$I_{in} = \left(\cosh\gamma l + \frac{Z_L}{Z_0}\sinh\gamma l\right) I_L \quad \text{or} \quad \frac{I_L}{I_{in}} = \frac{1}{\cosh\gamma l + \frac{Z_L}{Z_0}\sinh\gamma l} \tag{8}$$

which is Chipman's current equation apart from notation.

The ARRL voltage and current equations are obtained from (6) by similar steps. To obtain the ARRL voltage equation, we substitute the input constraint $I_{in} = E_{in}/Z_{in}$ into the equation given by the first row of (6), obtaining

$$E_L = \left(\cosh\gamma l - \frac{Z_0}{Z_{in}}\sinh\gamma l\right) E_{in} \quad \text{or} \quad \frac{E_L}{E_{in}} = \cosh\gamma l - \frac{Z_0}{Z_{in}}\sinh\gamma l \tag{9}$$

Similarly, the equation from the second row of (6) gives the ARRL current equation.

$$I_L = \left(\cosh\gamma l - \frac{Z_{in}}{Z_0}\sinh\gamma l\right) I_{in} \quad \text{or} \quad \frac{I_L}{I_{in}} = \cosh\gamma l - \frac{Z_{in}}{Z_0}\sinh\gamma l \tag{10}$$

Power Transmission Efficiency

Power efficiency η can be derived from any of (7) – (10). For example, using the current equations (8) and (10), efficiency is expressed in two equivalent forms as

$$\eta = \frac{P_L}{P_{in}} = \frac{|I_L|^2 R_L}{|I_{in}|^2 R_{in}} = \frac{R_L}{R_{in}} \frac{1}{\left|\cosh\gamma l + \frac{Z_L}{Z_0}\sinh\gamma l\right|^2} = \frac{R_L}{R_{in}} \left|\cosh\gamma l - \frac{Z_{in}}{Z_0}\sinh\gamma l\right|^2 \tag{11}$$

The voltage equations (7) and (9) give two more equivalent formulas for efficiency.

$$\eta = \frac{P_L}{P_{in}} = \frac{|E_L|^2 G_L}{|E_{in}|^2 G_{in}} = \frac{G_L}{G_{in}} \frac{1}{\left|\cosh\gamma l + \frac{Z_0}{Z_L}\sinh\gamma l\right|^2} = \frac{G_L}{G_{in}} \left|\cosh\gamma l - \frac{Z_0}{Z_{in}}\sinh\gamma l\right|^2 \tag{12}$$

Total Loss Factor

The power loss of a transmission line is commonly expressed as a factor greater than unity defined as the reciprocal of efficiency.

$$\text{Total Loss Factor} = \frac{P_{in}}{P_L} = \frac{1}{\eta} \tag{13}$$

By substituting the expressions for efficiency given in (11) and (12), we obtain four equivalent formulas for the loss factor of a terminated transmission line.

It should be mentioned that the loss formulas in the table are not being attributed to Chipman or the ARRL. Indeed the formulas do not appear in those works. The column labels note the starting points of the present analysis. All formulas in **Table 1** are equivalent, i.e. give the same result, and are general in that they are valid for complex values of γ, Z_0, and Z_L. In particular, the characteristic impedance need not be a real number. The only assumption is that the line is uniform so that γ and Z_0 are constants that do not vary with position along the line.

The formulas in Table 1 are multiplicative factors that relate input power to output power. It is customary to express loss in

Table 1 – Total Loss Factor of Terminated Transmission Lines.

Starting Equation Type	*ABCD Chain Matrix*	*Inverse ABCD Chain Matrix*
Current	$\frac{1}{\eta} = \frac{R_{in}}{R_L}\left\|\cosh\gamma l + \frac{Z_L}{Z_0}\sinh\gamma l\right\|^2$	$\frac{1}{\eta} = \frac{R_{in}}{R_L}\frac{1}{\left\|\cosh\gamma l - \frac{Z_{in}}{Z_0}\sinh\gamma l\right\|^2}$
Voltage	$\frac{1}{\eta} = \frac{G_{in}}{G_L}\left\|\cosh\gamma l + \frac{Z_0}{Z_L}\sinh\gamma l\right\|^2$	$\frac{1}{\eta} = \frac{G_{in}}{G_L}\frac{1}{\left\|\cosh\gamma l - \frac{Z_0}{Z_{in}}\sinh\gamma l\right\|^2}$

Table 2 – Total Loss of Terminated Line in Decibels.

Starting Equation Type	*ABCD Chain Matrix*	*Inverse ABCD Chain Matrix*
Current	$10\log_{10}\frac{R_{in}}{R_L}+20\log_{10}\left\lvert\cosh\gamma l+\frac{Z_L}{Z_0}\sinh\gamma l\right\rvert$	$10\log_{10}\frac{R_{in}}{R_L}-20\log_{10}\left\lvert\cosh\gamma l-\frac{Z_{in}}{Z_0}\sinh\gamma l\right\rvert$
Voltage	$10\log_{10}\frac{G_{in}}{G_L}+20\log_{10}\left\lvert\cosh\gamma l+\frac{Z_0}{Z_L}\sinh\gamma l\right\rvert$	$10\log_{10}\frac{G_{in}}{G_L}-20\log_{10}\left\lvert\cosh\gamma l-\frac{Z_0}{Z_{in}}\sinh\gamma l\right\rvert$

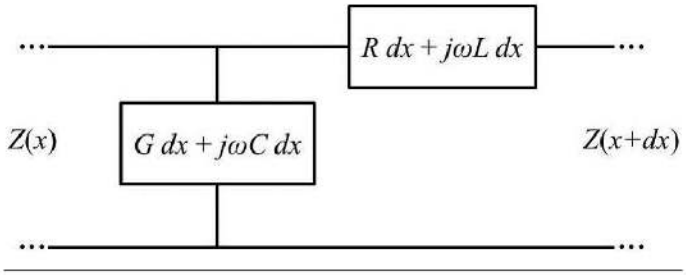

Figure 1 — Differential section of a transmission line.

decibel units, $10\times\log_{10}$ of the loss factor. **Table 2** gives the formulas expressed in decibels. The equations in the top row were first presented by the author at ARRL Pacificon 2014, **[7]**.

All of the formulas below involve the input resistance R_{in} or input conductance G_{in}, which are the real parts of the input impedance and admittance respectively. The input impedance depends on the load impedance according to

$$\begin{aligned} Z_{in} &= \frac{Z_L\cosh\gamma l \;+\; Z_0\sinh\gamma l}{\frac{Z_L}{Z_0}\sinh\gamma l \;+\; \cosh\gamma l} \\ &= Z_0\left(\frac{\frac{Z_L}{Z_0}\cosh\gamma l \;+\; \sinh\gamma l}{\frac{Z_L}{Z_0}\sinh\gamma l \;+\; \cosh\gamma l}\right) \end{aligned} \tag{14}$$

which is proved next. The input resistance and conductance are then given by

$$R_{in} = \mathrm{Re}\{Z_{in}\} \quad \text{and} \quad G_{in} = \mathrm{Re}\{Y_{in}\} = \mathrm{Re}\left\{\frac{1}{Z_{in}}\right\} \tag{15}$$

Impedance Transformation along a Line

Two methods for obtaining line impedance will be mentioned. The first is a simple derivation method that results in (14). Given the *ABCD* chain matrix (5), one writes

$$\begin{aligned} Z_{in} &= \frac{E_{in}}{I_{in}} \\ &= \frac{\left(\frac{E_L}{I_L}\right)\cosh\gamma l \;+\; Z_0\sinh\gamma l}{\left(\frac{E_L}{I_L}\right)\frac{1}{Z_0}\sinh\gamma l \;+\; \cosh\gamma l} \end{aligned} \tag{16}$$

from which (14) follows immediately. The second derivation method is novel because it bypasses the Telegrapher's equations. Consider the transmission line equivalent circuit model shown in **Figure 1** for a length dx of line having distributed parameters R, L, G, and C.

Considering only impedances seen looking to the right (toward increasing x), we write the impedance seen at $x + dx$ by removing the shunt and series terms respectively from the impedance seen at x.

$$\begin{aligned} Z(x)+dZ &= -\left(R+j\omega L\right)dx+\frac{1}{\frac{1}{Z(x)}-\left(G+j\omega C\right)dx} \\ &= -\left(R+j\omega L\right)dx+Z(x)\frac{1}{1-Z(x)\left(G+j\omega C\right)dx} \\ &= -\left(R+j\omega L\right)dx+Z(x)\left(1+Z(x)\left(G+j\omega C\right)dx\right) \\ &= Z(x)-\left[\left(R+j\omega L\right)-Z^2(x)\left(G+j\omega C\right)\right]dx \end{aligned} \tag{17}$$

which simplifies to a Ricatti differential equation

$$Z_0\frac{dZ}{dx} = -\gamma\left(Z_0^2 - Z^2(x)\right) \tag{18}$$

If the line is uniform, the distributed parameters are constant and (18) can be solved to obtain

$$\begin{aligned} Z(x) &= Z_0\tanh(-\gamma x+K) \\ &= Z_0\frac{-\tanh\gamma x \;+\; \tanh K}{1 \;-\; \tanh\gamma x\tanh K} \end{aligned} \tag{19}$$

K is a complex constant that satisfies the boundary condition at the load location $Z(x) = Z_L$. If the origin $x = 0$ is the load location, then

$$\tanh K = \frac{Z_L}{Z_0} \tag{20}$$

Substituting (20) into (19), the impedance function is found to be

$$\begin{aligned} Z(x) &= Z_0\frac{-\tanh\gamma x \;+\; \frac{Z_L}{Z_0}}{1 \;-\; \frac{Z_L}{Z_0}\tanh\gamma x} \\ &= Z_0\frac{\frac{Z_L}{Z_0}\cosh\gamma x \;-\; \sinh\gamma x}{-\frac{Z_L}{Z_0}\sinh\gamma x \;+\; \cosh\gamma x} \end{aligned} \tag{21}$$

Since $Z(x)$ is the impedance seen looking to the right, and the load is at $x = 0$, the input impedance is obtained by setting $x = -l$.

$$Z_{in} = Z(-l) = Z_0 \frac{\frac{Z_L}{Z_0}\cosh \gamma l + \sinh \gamma l}{\frac{Z_L}{Z_0}\sinh \gamma l + \cosh \gamma l} \tag{22}$$

which completes the proof of (14).

In the case of non-uniform line, the line parameters $R(x)$, $L(x)$, $G(x)$, $C(x)$, and hence $\gamma(x)$, and $Z_0(x)$, are functions of position. (18) becomes a general Ricatti equation

$$Z_0(x)\frac{dZ}{dx} = -\gamma(x)\left(Z_0^2(x) - Z^2(x)\right) \tag{23}$$

For tapered lines having certain tapers, analytic solution is possible.

Matched Loss

The matched impedance case ($Z_L = Z_0$) deserves special mention. In this case (14) shows the input impedance also equals the characteristic impedance ($Z_{in} = Z_0$). It follows that $Z_{in} = Z_L$, and hence that $R_{in} = R_L$ and $G_{in} = G_L$. Upon substituting these conditions into the formulas in Tables 1 and 2 and using the hyperbolic identities

$$\begin{aligned} \cosh \gamma l + \sinh \gamma l &= e^{\gamma l} = e^{\alpha} \cdot e^{j\beta} \\ \cosh \gamma l - \sinh \gamma l &= e^{-\gamma l} = e^{-\alpha} \cdot e^{-j\beta} \end{aligned} \tag{24}$$

the loss factor formulas in Table 1 simplify to the matched loss factor defined as

$$\text{Matched Loss Factor} = a = e^{2\alpha l} \ . \tag{25}$$

The Latin a and Greek α should not be confused. Greek α ($\alpha \geq 0$) is a nonnegative real number that represents the line's attenuation constant in nepers per unit length, whereas Latin a is a real number greater than or equal to unity ($a \geq 1$) and is the ratio of input to output power of the forward wave in a length l of line. a is dimensionless and represents the matched loss of the line when terminated in a matched load. In the case of an ideal lossless line, $\alpha = 0$ and $a = 1$.

Likewise, the formulas of Table 2 all simplify to the matched loss in decibels defined as

$$\begin{aligned} 10\log_{10} a &= 10\log_{10} e^{2\alpha l} \\ &= \left(20\log_{10} e\right) \times \alpha l \\ &= 8.6859 \times \alpha l \quad \text{dB} \end{aligned} \tag{26}$$

The constant 8.6859 converts the units of attenuation αl from nepers (Np) to decibels (dB), the conversion being 1 Np = 8.6859 dB.

Since we have defined loss factor as the reciprocal of efficiency, it will be convenient to define the matched efficiency as

$$\eta_{matched} = \frac{1}{a} = e^{-2\alpha l} \tag{27}$$

It can be shown that if Z_0 is real, as in the case of Heaviside line, the maximum efficiency is attained when the load is matched, and is

$$\eta_{max} = \eta_{matched} = \frac{1}{a} = e^{-2\alpha l} \tag{28}$$

However, this result is only true for real Z_0 and is not true in general if Z_0 is complex.

Additional Loss Due to SWR

The "Additional Loss Due to SWR" is the loss over and above the matched loss. It can be expressed as a factor or in decibels.

$$\text{Additional Loss Factor} = \frac{\text{Total Loss Factor}}{\text{Matched Loss Factor}} = \frac{1}{a\eta}$$

$$\begin{aligned} \text{Additional Loss (dB)} &= \text{Total Loss (dB)} - \text{Matched Loss (dB)} \\ &= 10\log_{10}\frac{P_{in}}{P_L} - 10\log_{10} a \\ &= \text{Total Loss (dB)} - 8.6859 \times \alpha l \ \text{(dB)} \end{aligned} \tag{29}$$

The formulas in Tables 1 and 2 are easily converted from total to additional loss by removing the matched loss from the total loss using the conversions given in (29).

Older Formulations for Loss

The circuit theory of transmission lines dates back to the 19th century and Oliver Heaviside, a reclusive Scottish genius who pioneered the subject. The subject developed in the 20th century as many university text books and research papers were published. See the **Biliography: Classic Works on Transmission Line Circuit Theory**.

The classic literature on transmission line circuit theory was searched for treatments of general lines that have complex characteristic impedance. Almost all authors treat the special case of Heaviside line. The majority of works treat only the case of real characteristic impedance. This is certainly true of publications in RF design engineering. See the **Sidebar: Heaviside Transmission Line**.

Considerably less has been written about general uniform line for which characteristic impedance is a complex number. Such matters concern not only electric power and telephone transmission systems, but also medical RF systems where knowledge of exact line loss and power levels is important to setting patient exposure for various treatments.

R.W.P. King (1943) distinguishes three different approaches to transmission line analysis, which he names "completely hyperbolic," "conventional hyperbolic," and "exponential," with the first being credited to A.E. Kennelly. Early writers including Kennelly, King, and Jackson used completely hyperbolic representations. Reading these early works requires knowledge of basic facts about hyperbolic trigonometric functions, including identities and relations to other functions which are found in standard handbooks [1], [2], [3]. Modern writers prefer the exponential or conventional hyperbolic approaches, which lead to longer formulas but fewer identities to remember.

Table 3 lists the known loss formulas for general transmission line. All claim generality, but no attempt was made to demonstrate equivalence among these formulas. The first ones listed are (11), which are proved above. Jackson's loss formula appears to be problematic for two reasons. First, Jackson's formula looks identical to King's low loss approximation, which is a special case derived from King's general formula. Second, the relevant complex hyperbolic angles are defined differently: Jackson uses hyperbolic tangent (tanh) where King uses hyperbolic cotangent (coth). This difference cannot be easily reconciled. It is also noted that Kennelly's formula differs from those of the author in certain respects. Further

Table 3 – Total Loss Factor of General Transmission Lines, Z_0 complex.

Author	*Total Loss Factor*	*Claims*
S.D. Stearns, K6OIK, ARRL Pacificon 2014 Eqn (11) and Table 1	$\frac{1}{\eta}=\frac{R_{in}}{R_L}\left\lvert\cosh\gamma l+\frac{Z_L}{Z_0}\sinh\gamma l\right\rvert^2$ $=\frac{R_{in}}{R_L}\frac{1}{\left\lvert\cosh\gamma l-\frac{Z_{in}}{Z_0}\sinh\gamma l\right\rvert^2}$	General, where $\gamma=\alpha+j\beta$
Eqn (12) or Table 1	$\frac{1}{\eta}=\frac{G_{in}}{G_L}\left\lvert\cosh\gamma l+\frac{Z_0}{Z_L}\sinh\gamma l\right\rvert^2$ $=\frac{G_{in}}{G_L}\frac{1}{\left\lvert\cosh\gamma l-\frac{Z_0}{Z_{in}}\sinh\gamma l\right\rvert^2}$	General, where $\gamma=\alpha+j\beta$
W.W. Macalpine, Trans. AIEE, July 1953, Eqn. 13	$\frac{1}{\eta}=\frac{1-\lvert\Gamma_{in}\rvert^2-2\lvert\Gamma_{in}\rvert\left(\frac{X_0}{R_0}\right)\sin 2\psi_{in}}{1-\lvert\Gamma_L\rvert^2-2\lvert\Gamma_L\rvert\left(\frac{X_0}{R_0}\right)\sin 2\psi_L}$	General, where $\Gamma=\lvert\Gamma\rvert e^{j2\psi}$
W. Jackson, 1945, eq. 4.30	$\frac{1}{\eta}=\frac{\sinh 2(\alpha l+u)}{\sinh 2u}$ $=\frac{(1+\coth 2u)e^{2\alpha l}+(1-\coth 2u)e^{-2\alpha l}}{2}$	Low loss approx. $\tanh(u+jv)=\frac{Z_L}{Z_0}$ $Z_0\approx R_0$
King, Mimno, Wing, 1945 pp. 69 and 293	$\frac{1}{\eta}=\frac{\sinh 2(\alpha l+\rho)}{\sinh 2\rho}$	Low loss approx. $Z_0\approx R_0$ and $\phi\approx 0$
R.W.P. King J.A.P., Nov. 1943, p. 593, eq. 84 and 1955, ch. 4, § 6, eq. 10	$\frac{1}{\eta}=\frac{\sinh 2(\alpha l+\rho)-\phi\sin 2(\beta l+\Phi)}{\sinh 2\rho-\phi\sin 2\Phi}$	General, where $\coth(\rho+j\Phi)=\frac{Z_L}{Z_0}$ $Z_0=R_0(1-j\phi)$
A.E. Kennelly, 1912 p. 117, eq. 202d	$\frac{1}{\eta}=\frac{R_{in}}{R_L}\left\lvert\frac{\sinh\gamma l+\frac{Z_L}{Z_0}\cosh\gamma l}{\tanh(\gamma l+\theta')}\right\rvert^2$	General, where $\tanh\theta'=\frac{Z_L}{Z_0}$

analysis is required to determine whether there is an error in Jackson or an older error in Kennelly that might have carried into King. It is known that the author's and Macalpine's formulas simplify to correct formulas in the case of real characteristic impedance.

Power Waves

Conventional traveling waves represent real power flow on a line only if the line's characteristic impedance is a real number. Conversely, if a line's characteristic impedance is complex, conventional traveling waves do not account for power flow correctly. In the case of complex Z_0, the real power flowing across a reference plane that divides the line is not the difference in the traveling wave real powers, $P_F - P_R$. Despite the failure of traveling waves to explain power flow correctly on lines having complex Z_0, there was desire for a "wave" interpretation that would explain delivered power crossing a reference plane as the difference between "forward" power and "reverse" power. Power waves were introduced for this purpose. Early work on power waves by Youla (1961) and Kurokawa (1965) introduced the waves as fictitious mathematical contrivances. Kurokawa wrote that power waves as he defined them are neither physical nor unique. The waves are just one of an infinite number of choices of "pseudo-waves" that can explain power flow on a line.

Rahola (2008) showed that Youla-Kurokawa pseudo-waves do have a special property. They are consistent with real power flow and real power transfer through 2-port networks, and simultaneous conjugate matching at two ports. Despite these features, Youla-Kurokawa power waves give wrong values for reactive and complex power. So their designation as fictitious pseudo-waves remained. In a 2016 paper, R.H. Johnston and M. Okoniewski showed that a modification to Kurokawa's definition, a different one of the infinite number of choices, gives correct values for reactive as well as real power. To distinguish the new power waves from the old Youla-Kurokawa ones, the term "new power wave" was introduced. New power waves appear to be unique among the infinite set of pseudo-waves considered by Kurokawa. They retain the conjugate match properties pointed out by Rahola but also give correct values of real and reactive delivered power when reverse power is subtracted from forward power.

Table 4 gives the definitions of the different wave types in terms of line voltage and current. Reactive powers of the waves, Q_F and Q_R,

Table 4 – Wave Definition Summary Table.

Type	*Conventional Traveling Waves*	*Normalized Traveling Waves*	*Youla-Kurokawa Power Waves*	*Johnston-Okoniewski New Power Waves*
Forward Wave	$V_F(x)=\frac{1}{2}\left(V(x)+Z_0 I(x)\right)$ $I_F(x)=\frac{1}{2}\left(\frac{V(x)}{Z_0}+I(x)\right)$	$a(x)=\frac{V(x)+I(x)Z_0}{2\sqrt{\mathrm{Re}\{Z_0\}}}$	$a(x)=\frac{V(x)+I(x)Z_0}{2\sqrt{\mathrm{Re}\{Z_0\}}}$	$a(x)=\frac{1}{2}\left(V(x)\sqrt{Y_0^*}+I(x)\sqrt{Z_0}\right)$
Reverse Wave	$V_R(x)=\frac{1}{2}\left(V(x)-Z_0 I(x)\right)$ $I_R(x)=\frac{1}{2}\left(\frac{V(x)}{Z_0}-I(x)\right)$	$b(x)=\frac{V(x)-I(x)Z_0}{2\sqrt{\mathrm{Re}\{Z_0\}}}$	$b(x)=\frac{V(x)-I(x)Z_0^*}{2\sqrt{\mathrm{Re}\{Z_0\}}}$	$b(x)=\frac{1}{2}\left(V(x)\sqrt{Y_0^*}-I(x)\sqrt{Z_0}\right)$
Wave Real Power	$P_F=\frac{1}{2}\mathrm{Re}\{V_F I_F^*\}$ $P_R=\frac{1}{2}\mathrm{Re}\{V_R I_R^*\}$	$P_F=\lvert a(x)\rvert^2$ $P_R=\lvert b(x)\rvert^2$	$P_F=\lvert a(x)\rvert^2$ $P_R=\lvert b(x)\rvert^2$	$P_F=\lvert a(x)\rvert^2$ $P_R=\lvert b(x)\rvert^2$
Delivered Complex Power, P + jQ, (toward load)	$P(x)=P_F-P_R$ $+\frac{1}{4}\left(V_F V_R^*-V_F^* V_R\right)\left(\frac{1}{Z_0}-\frac{1}{Z_0^*}\right)$	$P(x)=\lvert a(x)\rvert^2-\lvert b(x)\rvert^2$ + extra terms	$P(x)=\lvert a(x)\rvert^2-\lvert b(x)\rvert^2$ $Q(x)=j\left(ab^*-a^*b\right)$ + extra terms	$P(x)=\lvert a(x)\rvert^2-\lvert b(x)\rvert^2$ $Q(x)=j\left(ab^*-a^*b\right)$
Reflection Coefficient at Load	$\Gamma_L=\frac{Z_L-Z_0}{Z_L+Z_0}$	$\Gamma_L=\frac{Z_L-Z_0}{Z_L+Z_0}$	$\Gamma_L=\frac{Z_L-Z_0^*}{Z_L+Z_0}$	$\Gamma_L=\frac{Z_L-\lvert Z_0\rvert}{Z_L+\lvert Z_0\rvert}$

are not given but are defined like the real powers P_F and P_R except as an imaginary part. The difference $Q_F - Q_R$, is $Q(x)$, the reactive part of complex power delivered at x. The main thing to note is for new power waves the difference between forward and reverse complex (real and reactive) wave powers agree with delivered complex power at every point along a transmission line.

Standing Wave Ratio

The difference between SWR and VSWR is the initial 'V' which stands for voltage. The V was dropped by ARRL in the 1990s to recognize that VSWR and ISWR are the same. Traveling waves give rise to voltage and current standing waves, and both types have the same SWR. This statement remains true even if Z_0 is complex. This is a statement about SWR, not about formulas for SWR. Formulas must be changed or generalized, for complex Z_0.

Power waves and new power waves are pseudo waves. They are linear combinations of voltage and current on the line and hence linear combinations of voltage and current traveling waves. They give rise to a different kind of standing wave, properly called a pseudo standing wave. Most SWR meters measure VSWR or ISWR and call it SWR. [SWR meters usually measure reflection coefficient magnitude and relate it to a graphical solution for SWR on the meter face presentation — *Ed.*]. No meter measures PWSWR or NPWSWR. Perhaps someday you will be able to buy a meter that measures these new parameters, but for now we will be satisfied with formulas for VSWR that are applicable when Z_0 is complex.

Reflection coefficients for power waves or new power waves or other pseudo-waves should not be used to compute SWR because we want VSWR or ISWR not PWSWR. In other words, we want the standing wave ratio of a certain kind of standing wave – the voltage or current standing wave. SWR formulas valid for real Z_0 can give negative values as Paradox 2 shows. A general SWR formula is needed, one that is valid for arbitrary complex Z_0.

To obtain a general formula for voltage standing wave ratio, we start with the voltage from (7).

$$E(x)=\left(\cosh\gamma x+\frac{Z_0}{Z_L}\sinh\gamma x\right)E_L \tag{30}$$

where x is distance measured from the load. Upon expanding this equation, we separate the voltage into its traveling wave components.

$$\begin{aligned}\frac{E(x)}{E_L}&=\left(\frac{e^{\gamma x}+e^{-\gamma x}}{2}\right)+\frac{Z_0}{Z_L}\left(\frac{e^{\gamma x}-e^{-\gamma x}}{2}\right)\\&=\frac{e^{\gamma x}}{2}\left(1+\frac{Z_0}{Z_L}\right)+\frac{e^{-\gamma x}}{2}\left(1-\frac{Z_0}{Z_L}\right)\\&=e^{j\beta x}\left(\frac{e^{\alpha x}}{2}\right)\left(1+\frac{Z_0}{Z_L}\right)+e^{-j\beta x}\left(\frac{e^{-\alpha x}}{2}\right)\left(1-\frac{Z_0}{Z_L}\right)\end{aligned} \tag{31}$$

The voltage can be interpreted as the sum of two phasors that counter-rotate as x varies. Voltage standing wave ratio is defined in terms of the lengths of these phasors, which are complex numbers. Similar to Chipman's analysis for the real Z_0 case, we define VSWR at x as the ratio of upper to lower envelopes of the voltage along the line [4, pp. 167-171]. The ratio of the maximum to minimum that these lengths can sum to is

$$\begin{aligned}\mathrm{VSWR}&=\frac{\max\limits_{\phi}\left|\left(\frac{e^{\alpha x}}{2}\right)\left(1+\frac{Z_0}{Z_L}\right)+e^{j\phi}\left(\frac{e^{-\alpha x}}{2}\right)\left(1-\frac{Z_0}{Z_L}\right)\right|}{\min\limits_{\psi}\left|\left(\frac{e^{\alpha x}}{2}\right)\left(1+\frac{Z_0}{Z_L}\right)+e^{j\psi}\left(\frac{e^{-\alpha x}}{2}\right)\left(1-\frac{Z_0}{Z_L}\right)\right|}\\&=\frac{e^{\alpha x}\left|1+\frac{Z_0}{Z_L}\right|+e^{-\alpha x}\left|1-\frac{Z_0}{Z_L}\right|}{\left|e^{\alpha x}\left|1+\frac{Z_0}{Z_L}\right|-e^{-\alpha x}\left|1-\frac{Z_0}{Z_L}\right|\right|}\\&=\frac{1+e^{-2\alpha x}\left|\Gamma_L\right|}{\left|1-e^{-2\alpha x}\left|\Gamma_L\right|\right|}\\&=\left|\frac{1+\left|\Gamma(x)\right|}{1-\left|\Gamma(x)\right|}\right|\end{aligned} \tag{32}$$

From the last line we see that the VSWR formula for complex Z_0 is almost the same as that for real Z_0. VSWR at x depends on the traveling wave reflection coefficient at x and is computed as the absolute value of the formula for SWR assuming real Z_0. The only difference between (32) and the conventional VSWR formula for real Z_0 is that one must take the absolute value of the denominator. This ensures the ratio is positive. A derivation based on current leads to the same formula for ISWR. Hence we may continue to use SWR for both VSWR and ISWR.

Return Loss

Return Loss is a commonly used parameter in RF design and transmission systems and is used as a measure of impedance matching and standing wave ratio. The concept of return loss originated with the idea of forward and reverse traveling waves and the standing waves created therefrom. Recently, however, return loss has been extended to general circuit junctions that have no transmission lines or waves. In terms of waves on a transmission line, return loss is fundamentally a measure of power delivery to a load. One conceptual definition is

$$\begin{aligned}\text{Return Loss} &= \frac{\text{Re}\{S_F\}}{\text{Re}\{S_R\}} \\ &= \frac{\text{Re}\{P_F + jQ_F\}}{\text{Re}\{P_R + jQ_R\}} \\ &= \frac{P_F}{P_R}\end{aligned} \tag{33}$$

where P, Q, and S denote real, reactive, and complex power respectively, and the subscripts indicate the direction of the waves as forward (toward the load) or reverse (away from the load). All quantities vary with position along a transmission line. In (33), return loss depends only on wave type and reflection at the load but not on source or generator impedance.

A different concept of return loss can be stated without wave ideas purely in terms of circuit impedances. Consider a generator with a series impedance connected to a load impedance. Camacho-Peñalosa and Baños-Polglase define return loss formally as the ratio of available generator power to power not delivered to the load **[8]**. If the power delivered to the load is a fraction M of the available power, then the fraction of available power not delivered to the load is $1-M$ and, therefore, return loss is $1/(1-M)$.

$$\text{Return Loss} = \frac{1}{1-M} \tag{34}$$

Although this definition does not involve waves, it nonetheless can be applied to transmission lines by defining a junction as a reference plane that divides a line. If a reference plane is placed at some point along the line, the return loss at that point can be defined in terms of the impedances seen looking from reference plane toward the source and toward the load. Toward the source, we see a Thévenin equivalent source; whereas, toward the load we see the transformed load impedance given by (14). Thus the transmission line is replaced by two impedances Z_1 and Z_2, which are the Thévenin source impedance and transformed load impedance respectively. Return loss is now found from (34) to be

$$\text{Return Loss} = \frac{1}{1-M} = \frac{|Z_1 + Z_2|^2}{|Z_1 + Z_2|^2 - R_1 R_2} \tag{35}$$

An unusual property of this definition of return loss is that it depends on the source impedance. There is another definition of return loss that depends on source impedance. The IEEE Standard Dictionary gives a six-part definition of return loss. In one IEEE definition, return loss is defined as a measure of the dissimilarity of the two impedances Z_1 and Z_2 at a junction.

$$\text{Return Loss} = \left|\frac{Z_1 + Z_2}{Z_1 - Z_2}\right|^2 \tag{36}$$

Equations (35) and (36) define return loss without reference to Z_0. A criticism of the IEEE definition (36) is that if the angle between Z_1 and Z_2 is obtuse, the return loss is sub-unity (negative dB). Camacho-Peñalosa and Baños-Polglase claim that (35) implies (36). However their proof is defective. A simple proof that (35) and (36) are not equivalent is to note that the return loss given by (35) is greater than or equal to unity, whereas that given by (36) is merely nonnegative. A sub-unity value for (35) is not possible. Nonequivalence can also be proved by counterexample. Let the source be matched to the line, such that $Z_g = Z_0 = Z_1$. Then (35) simplifies to the return loss formula for the Youla-Kurokawa power wave, while (36) simplifies to the return loss formula for conventional traveling waves. Numerical examples below show this.

We will compare five different definitions of return loss. Four different formulas for return loss can be expressed in terms of impedances: three from the last row of Table 4, plus one from circuit theory. The fourth depends on source impedance. A matched source $Z_g = Z_0$ is assumed.

Table 5 lists return loss formulas. We compare these formulas by using examples. In **Figures 2 and 3** the frequency is 1 MHz, and the load is a complex impedance $Z_L = 1 - j75\ \Omega$. The line parameters are similar to those of RG-174 coax. In Figure 2, $Z_0 = 55.86 - 3.824\ \Omega$, velocity factor is 0.66, and the line length from source to load is 600 feet or 0.924 wavelengths. The abscissa measures distance in feet from the load toward the source. The source is to the left

Table 5 – Four different formulas for return loss can be

Conventional	$\text{RL} = \left\|(Z_2 + Z_0)/(Z_2 - Z_0)\right\|^2$
Youla-Kurokawa power wave	$\text{RL} = \left\|(Z_2 + Z_0)/(Z_2 - Z_0^*)\right\|^2$
Johnston new power wave	$\text{RL} = \left\|(Z_2 + \|Z_0\|)/(Z_2 - \|Z_0\|)\right\|^2$
Camacho-Peñalosa	$\text{RL} = \left\|(Z_2 + Z_0)\right\|^2 / \left[\left\|(Z_2 + Z_0)\right\|^2 - 4R_2R_0\right]$

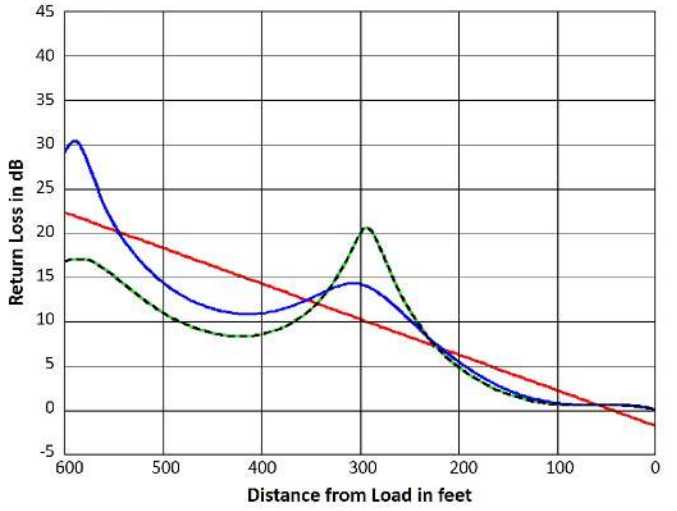

Figure 2 — Comparison of four definitions of return loss for complex Z_0. Referring to the left side of the chart, the top most curve is the "Johnston new power wave," the straight line is a "Conventional travelling wave," the dashed line is "C.-Peñalosa available power," which overlays the "Youla Kurokawa power wave" curve.

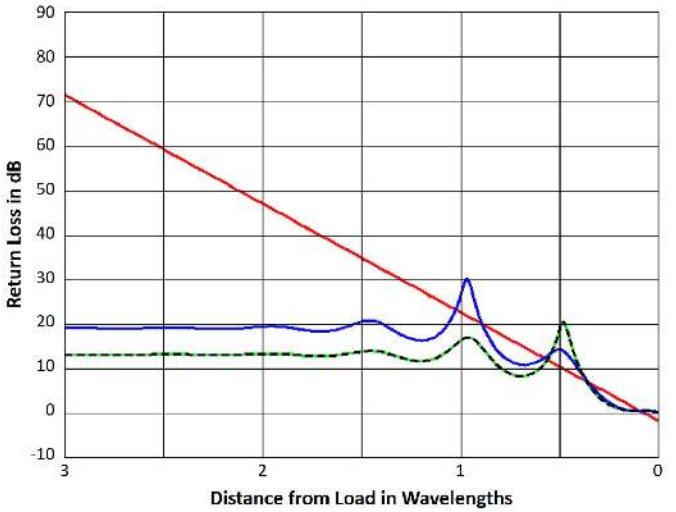

Figure 3 — Extended graphs comparing four definitions of return loss. Referring to the left side of the chart, the top most straight line is a "Conventional travelling wave" curve below it is "Johnston new power wave," the dashed line is "C.-Peñalosa available power," which overlays the "Youla Kurokawa power wave" curve.

and the load at the right edge of the graph. Figure 3 is for a similar line whose length is about three times as long. $Z_0 = 53.42 - j11.86$ Ω, and velocity factor is 0.6181. The abscissa measures distance in wavelengths from the load out to 3 wavelengths.

The figures reveal several interesting things. First, the return loss computed from conventional traveling waves is sub-unity (negative dB) near the load. Second, the return loss computed by the other three approaches is always greater than unity (positive dB) but is not monotonic with distance. Johnston new power wave return loss tends to track the conventional traveling wave return loss, fluctuating equally above and below the latter.

Third, the Youla-Kurokawa return loss and Camacho-Peñalosa return loss curves coincide exactly. The agreement depends on the fact that the source generator impedance is matched to the line. Camacho-Peñalosa return loss comes from circuit theory, not wave theory. Its use of the term "return loss" is artificial. If the generator is not impedance matched to the line, the Camacho-Peñalosa and Youla-Kurokawa curves will not coincide.

Fourth, Figure 3 shows that as the distance from the load increases, the influence of the load decreases. Moving away from the load, traveling wave return loss increases without bound, but the other return loss curves converge to a finite limit. This phenomenon is 'self-reflection' whereby the numerator of the reflection coefficient is not zero even if the line is terminated with a matched impedance load. In power wave theory, even an infinite line of complex Z_0 has both forward and reverse waves. The reverse wave is the result of continuous, distributed reflection that occurs along the entire length of the line. The flattening and convergence of the Camacho Peñalosa curve is due to the matched source assumption. If the source were not matched, this curve would agree with Youla-Kurokawa on the right side of the graph, extending from the load to the flat middle region. On the left side of the graph, near the source, the Camacho Peñalosa curve would exhibit variations. In fact, if the generator and load impedances are equal, $Z_g = Z_L$, the Camacho Peñalosa curve exhibits left-right mirror symmetry as is evident from the symmetric form of (35).

Finally, the limiting values of return loss differ between Johnston new power waves and Youla-Kurokawa power waves by a factor of 4 or 6 dB. The reason is that at great distance from the load Z_2

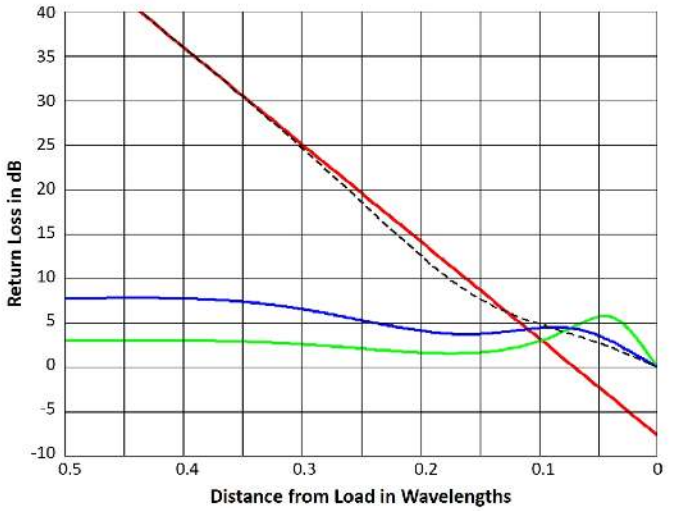

Figure 4 — A new definition of return loss for complex Z_0 lines proposed by W. Harriman. Referring to the left side of the chart, the top most solid curve is the "Conventional traveling wave," the dash line is the new "Proposed return loss definition," the next-lower solid line is the "Johnston new power wave," and the lowest line is the "Youla Kurokawa power wave."

converges to Z_0. If Z_0 is almost real, then:

$$\left|Z_0 - Z_0^*\right|^2 \approx 4\left|Z_0 - \left|Z_0\right|\right|^2.$$

The 6-dB offset is, therefore, an asymptotic result for almost real Z_0 but has no other special significance. The self-reflection phenomenon is less pronounced for Johnston new power waves than for Youla-Kurokawa power waves. In other words, the continuous distributed reflections are smaller.

A new definition of return loss was recently proposed by W. Harriman, AE6TY, and incorporated into his *SimSmith* software. **Figure 4** compares this return loss with the others mentioned so far.

Again the line is RG-174 but now at a frequency of 1 kHz. At this frequency the distributed series resistance R and shunt capacitance C dominate, and the distributed series inductance L and shunt conductance G are negligible. The line is basically series R and shunt C, and Z_0 is $793 - j791\ \Omega$, giving an impedance phase angle of –44.93°, which is near the lower limit of –45°. The load impedance Z_L is $1 + j110\ \Omega$. The magnitude of the voltage reflection coefficient at the load is $|\Gamma_L| = 2.406$, which is near the upper limit of 2.414. The abscissa extends to one-half wavelength measured from the load.

The proposed new return loss definition is

$$\begin{aligned}\text{Return Loss} &= \frac{P_{Delivered} + P_R}{P_R} \\ &= 1 + \frac{P_{Delivered}}{P_R}\end{aligned} \tag{37}$$

where $P_{Delivered}$ is delivered real power. Definition (37) can be expressed equivalently in terms of traveling wave voltages.

$$\begin{aligned}\text{Return Loss} &= \frac{P_F + \frac{1}{4}\left(V_F V_R^* - V_F^* V_R\right)\left(Y_0 - Y_0^*\right)}{P_R} \\ &= \frac{\frac{1}{2}|V_F|^2 G_0 + \frac{1}{2}\left(V_F V_R^* - V_F^* V_R\right) jB_0}{\frac{1}{2}|V_R|^2 G_0}\end{aligned} \tag{38}$$

In the case of complex Z_0, (37) shows that this return loss equals unity plus a positive quantity. Hence it is never sub-unity. In the case of real Z_0, (38) shows that the terms after the first in the numerator are zero because susceptance B_0 is zero, and the numerator is then just the forward traveling wave power. Hence the definition agrees with the conventional traveling wave return loss. Otherwise the second term in the numerator is the product of two imaginary numbers and is therefore real. The sign of this term alternates every quarter wavelength along the line, which causes the new return loss curve to vary above and below the conventional return loss curve as position varies along the line. Figure 4 shows this variation with position along a mismatched, lossy, non-Heaviside line. A key feature is the absence of convergence to a fixed value far from the load. The new return loss does not have a limiting value like power waves and new power waves. On this point we note the converged limits for power waves and new power waves differ by 4 dB. The decrease from 6 dB noted earlier is because the phase angle of Z_0 is greater at 1 kHz than at 1 MHz.

The graphs above show that, in general, different definitions of return loss give different results. In the end, choosing a definition is hard because it involves power. A similar situation exists in electromagnetic theory with the Poynting vector. $\mathbf{S} = \mathbf{E} \times \mathbf{H}$ represents power density flow through space. However, one can add any solenoidal field to $\mathbf{S}$ and get a different field that also explains power flow through space. Hence $\mathbf{S}$ is not unique. With transmission lines, we are dealing with power flow on lines. Although power waves can explain power flow, they are not unique. There is an arbitrariness in choosing a pseudo-wave.

Paradox 4: Anti-Matched Lines

This paper started with three paradoxes that might be called 'complex Z_0' paradoxes. They are not true paradoxes but merely puzzles that occur when one applies formulas that assume Z_0 is real when it is complex. The resolutions were explained above. We finish with a fourth paradox that is more difficult – one that occurs when Z_0 is real. This paradox is not a simple puzzle of using a right formula in a wrong way. The paradox arises in evaluating the voltage or current on a line that has an unusual load impedance.

Consider a uniform Heaviside transmission line of length l. We assume the line satisfies the Heaviside cross-ratio condition at all frequencies. The line may be lossy but it is dispersionless, distortionless, and has real Z_0. Let the line be terminated in the negative of its characteristic impedance, i.e. $-Z_0$. This load condition is an "anti-match." Since Z_0 is real, the load can be an ideal lumped-element negative resistor whose value is $-R_0$. Alternatively, we could start with one end of an infinite length of line, cut the line at length l from the end, and insert a 2-port negative impedance converter (NIC) between the finite section and the infinite remainder of the line.

Now suppose a voltage $e_{in}(t)$ is applied at the line's input end. The question is what is the voltage waveform $e_L(t)$ at the load? A more general question is, what is the voltage waveform $e(x, t)$ at location x along the line? We answer the former and leave the latter as an exercise for the reader.

The problem is to determine time-domain voltages. Starting from the frequency-domain formula (7), we have

$$\begin{aligned}E_L(\omega) &= \frac{E_{in}}{\left(\frac{e^{\gamma l} + e^{-\gamma l}}{2}\right) - \left(\frac{e^{\gamma l} - e^{-\gamma l}}{2}\right)} \\ &= E_{in}\, e^{\gamma l} \\ &= E_{in}\, e^{\alpha l} e^{j\beta l} \\ &= E_{in}(\omega)\, e^{\alpha l} e^{\frac{j\omega l}{v_f c}} \\ &= E_{in}(\omega)\, e^{\alpha l} e^{j\omega\tau}\end{aligned} \tag{39}$$

where v_f is velocity factor, c is the speed of light, and τ is the time delay of length l of the line. In order to interpret (39) in the time domain, we convert to the time domain by using the inverse Fourier transform or time shifting theorem to obtain

$$\begin{aligned}e_L(t) &= \Im^{-1} E_L(\omega) \\ &= \Im^{-1} E_{in}(\omega)\, e^{\alpha l} e^{j\omega\tau} \\ &= \frac{e^{\alpha l}}{2\pi} \int_{-\infty}^{\infty} E_{in}(\omega)\, e^{j\omega\tau} e^{j\omega t} d\omega \\ &= \left(\frac{e^{\alpha l}}{2\pi}\right) e_{in}(t + \tau)\end{aligned} \tag{40}$$

Again, $\tau = l/(v_f c)$ is the time delay associated with the length l of the line. Hence, the load voltage waveform is an amplitude-scaled, *time-advanced* replica of the input voltage. In plain terms, the output voltage is the future value of the input voltage. The anti-matched line is a *predictor*. Moreover, the longer the line, the farther into the future the circuit predicts. The line's delay $\tau = l/(v_f c)$ determines how far into the future the anti-matched line predicts!

The load current is obtained similarly. Starting with (8), we obtain

$$i_L(t) = \left(\frac{e^{\alpha l}}{2\pi}\right) i_{in}(t + \tau) \tag{41}$$

The circuit described here violates the fundamental principle of causality: An effect cannot precede its cause. Physical systems cannot behave this way. In these examples, we aren't considering

different observers, who can disagree on the time order of events due to special relativity. So, where does the problem lie? Only two assumptions were made: (a) the line is ideal Heaviside line, and (b) the termination is an ideal negative resistor. As an aside, the value of Z_0 need not be known, for we could have cut an infinite length of the line, and inserted an ideal negative impedance converter to convert Z_0 to $-Z_0$ without knowing the values involved. This latter method has the advantage that if Z_0 varies with frequency, the load impedance compensates perfectly, which is all (39) requires. So what is the source of the problem?

The time prediction paradox arises due to the anti-match termination $Z_L = -Z_0$. Now suppose the transmission line is negative and the load is positive. More precisely, suppose the real part of Z_0 is negative and the real part of Z_L is positive. Again the paradox rears its head. How does such a transmission line occur? You can build one as a ladder network of T or π sections in which the lumped reactances are non-Foster elements, viz. series negative inductors and shunt negative capacitors. Such elements can be realized by active circuits, and such transmission lines are the building blocks of the transmission line matrix (TLM) approach to making active metamaterials. Such materials can be double negative (DNG) or negative refractive index (NRI) or other types. In electromagnetic field theory similar paradoxes exist. Uniform plane waves incident on, or traveling inside, a Veselago/Pendry slab lens made of various kinds of metamaterials can seem to violate causality. Detailed analysis usually reveals backward waves in the metamaterial in which a wave's phase velocity vector points opposite to its energy velocity vector. However, Paradox 4 as given here does not occur in strange media, it occurs in an ordinary transmission line that satisfies Heaviside's conditions and is terminated with a strange load.

The anti-match, time prediction paradox is alarming because so few assumptions are made about the circuit elements involved. The only explanation of the paradox is that we have assumed ideal mathematical models for both the line and the load. Physical transmission line can at best only approximate ideal Heaviside line. Physical negative resistance devices and circuits can at best only approximate ideal negative resistors or ideal negative impedance converters. Physical devices may match the ideal models over many decades of bandwidth, but that is not good enough to ensure the violations of causality implied by (40) or (41).

Suppose, however, we forget about imperfect physical devices and consider circuit simulators instead. Surely anyone can make a circuit simulation model that uses the exact equations of the ideal devices posited above, valid over enormous bandwidth, that runs in double or quadruple precision. Might one be able to input a time series of stock market price data and peek ahead by a day or two? This method substitutes circuit simulation of an ideal transmission line for an imperfect physical one. No doubt upon reading this, some readers who have circuit simulators at their disposal will be tempted to do the experiment. If any readers succeed and become rich, please remember from whom you got the idea. And, if any other readers are motivated to learn and improve their skills at *SPICE* or *ADS* or *Microwave Office* (*MWO*) or *QucsStudio*, the author will consider that to be good and worthy compensation for having written this paper.

Acknowlegments

The author wishes to thank Ward Harriman, AE6TY, and Dan Maguire, AC6LA, for the discussions that led to the writing of this paper. The author is indebted to Dan Maguire for the examples and computing the graphs, which was done using the latest version of *SimSmith*.

Steve Stearns, K6OIK, started in ham radio while in high school at the height of the Heathkit era. He holds an Amateur Extra and an FCC commercial General Radio Operator license with Radar endorsement. He previously held Novice, Technician, and First Class Radiotelephone licenses. He studied electrical engineering at California State University Fullerton, the University of Southern California, and Stanford, specializing in electromagnetics, communication engineering and signal processing. Steve was a Technical Fellow of Northrop Grumman Corporation before retirement. He worked at Northrop Grumman's Electromagnetic Systems Laboratory in San Jose, California, where he led the development of advanced communication signal processing systems, circuits, antennas, and electromagnetic devices. Steve is Vice-President of the Foothills Amateur Radio Society, and served previously as Assistant Director of ARRL Pacific Division under Jim Maxwell, W6CF. He has over 80 professional publications and ten patents. Steve has received numerous awards for professional and community volunteer activities.

References

[1] M. Abramowitz and I. A. Stegun, editors, *Handbook of Mathematical Functions*, National Bureau of Standards.

[2] I.S. Gradshteyn and I.M. Ryzhik, *Table of Integrals, Series, and Products*, 7th ed., Academic Press, 2007.

[3] D. Zwillinger, editor, *CRC Standard Mathematical Tables and Formulae*, 30th ed., CRC Press, 1996.

[4] R.A. Chipman, *Theory and Problems of Transmission Lines*, McGraw-Hill, 1968. Page 155.

[5] H.W. Silver, NØAX, ed., *The ARRL Antenna Book for Radio Communication*, 24th ed., American Radio Relay League, 2019. Page 23-19.

[6] S. Ramo, J.R. Whinnery, and T. van Duzer, *Fields and Waves in Communication Electronics*, Wiley, 1967. Pages 605 and 609-612.

[7] S.D. Stearns, K6OIK, "A Transmission Line Power Paradox and Its Resolution," ARRL Pacificon Antenna Seminar, Oct. 10, 2014, p.43, **www.fars.k6ya.org/docs/k6oik#PowerParadox**.

[8] C. Camacho-Peñalosa and J.D. Baños-Polglase, "On the Definition of Return Loss," *IEEE Antennas and Propagation Magazine*, vol. 55, no. 2, pp. 172-174, Apr. 2013.

Bibliography: (most recent first) Power Wave Theory for General Transmission Lines

S. Amakawa, "Scattered Reflections on Scattering Parameters: Demystifying Complex-Referenced S Parameters," *IEICE Trans. Electronics* (Japan), vol. E99-C, no. 10, pp. 1100-1112, Oct. 2016.

R.H. Johnston and M. Okoniewski, "Propagation of New Power Waves On a Complex Impedance Transmission Line," *IEEE Int. Symp. Antennas and Propagation*, Fajardo, Puerto Rico, June 26-July 1, 2016.

D. Williams, "Traveling Waves and Power Waves: Building a Solid Foundation for Microwave Circuit Theory," *IEEE Microwave Magazine*, pp. 38-45, Nov/Dec. 2013.

S. Llorente-Romano, A. Garca-Lampérez, T.K. Sarkar, and M. Salazar-Palma, "An Exposition on the Choice of the Proper *S* Parameters in Characterizing Devices Including Transmission Lines with Complex Reference Impedances and a General Methodology for Computing Them," *IEEE Antennas and Propagation Magazine*, vol. 55, no. 4, pp. 94-112, Aug. 2013.

J. Rahola, "Power Waves and Conjugate Matching," *IEEE Trans. Circuits and Systems*, vol. 55, no. 1, pp. 92-96, Jan. 2008.

D.F. Williams and B.K. Alpert, "Characteristic Impedance, Power, and Causality," *IEEE Microwave and Guided Wave Letters*, vol. 9, no. 5, pp. 181-182, May 1999.

K. Kurokawa, "Power Waves and the Scattering Matrix," *IEEE Trans. Microwave Theory and Techniques*, vol. 13, no. 2, pp. 194-202, Mar. 1965.

D.C. Youla, "An Extension of the Concept of Scattering Matrix," *IEEE Trans. Circuit Theory*, vol. 11, no. 2, pp. 310-312, June 1964.

D.C. Youla and P.M. Paterno, "Realizable Limits of Error for Dissipationless Attenuators in Mismatched Systems," *IEEE Trans. Microwave Theory and Techniques*, vol. 12, no. 3, pp. 289-299, May 1964.

D.C. Youla, "On Scattering Matrices Normalized to Complex Port Numbers," *Proc IRE*, vol. 49, no. 7, p. 1221, July 1961.

P. Penfield, Jr., "Noise in Negative-Resistance Amplifiers," *IRE Trans. Circuit Theory*, vol. 7, no. 2, pp. 166-170, June 1960.

S.D. Stearns, K6OIK, "A Transmission Line Power Paradox and Its Resolution," *ARRL Pacificon Antenna Seminar*, Oct. 10, 2014, **www.fars.k6ya.org/docs/k6oik#PowerParadox**.

S.D. Stearns, K6OIK, "Facts about SWR and Loss," *ARRL Pacificon Antenna Seminar*, Oct. 15, 2010, **www.fars.k6ya.org/docs/k6oik#SWRandLoss**.

D. Maguire, AC6LA, "Additional Loss Due to SWR is in Quotes for a Reason," **https://www.ac6la.com/swrloss.html**.

O. Duffey, VK1OD, "Graphic demonstration of loss under standing waves," **https://owenduffy.net/blog/?p=6327**.

Bibliography: Classic Works on Transmission Line Circuit Theory

T.M. Papazoglou, "Review of the Maximum Efficiency of Transmission Lines," *IEEE Trans. Education*, vol. 35, no. 4, pp. 307-310, Nov. 1992.

R.J. Vernon and S.R. Seshadri, "Reflection Coefficient and Reflected Power on a Lossy Transmission Line," *Proc. IEEE*, vol. 57, no. 1, pp. 101-102, Jan. 1969.

R.A. Chipman, *Theory and Problems of Transmission Lines*, McGraw-Hill, 1968.

G.E. Stannard, "Calculation of Power on a Transmission Line," *Proc. IEEE*, vol. 55, no. 1, p. 132, Jan. 1967.

J.L. Stewart, *Circuit Analysis of Transmission Lines*, Wiley, 1958.

H.P. Westman, editor, *Reference Data for Radio Engineers*, 4th ed., ITT, 1956. Pages 564-566.

R.W.P. King, *Transmission Line Theory*, McGraw-Hill, 1955; Dover 1965.

W.W. Macalpine, "Transmission-Line Impedance and Efficiency," *Electrical Engineering*, vol. 72, no. 10, p. 868, Oct. 1953.

W.W. Macalpine, "Computation of Impedance and Efficiency of Transmission Line with High Standing-Wave Ratio," *Trans. AIEE*, vol. 72, no. 3, pp. 334-339, July 1953.

S.G. Lutz, "Transmission Line Load Impedance for Maximum Efficiency," *Trans. AIEE*, vol. 70, no. 1, pp. 283-285, July 1951.

H.H. Skilling, *Electric Transmission Lines*, McGraw-Hill, 1951.

W.C. Johnson, *Transmission Lines and Networks*, McGraw-Hill, 1950.

J.J. Karakash, *Transmission Lines and Filter Networks*, Macmillan, 1950.

W.W. Macalpine, "Heating of Radio-Frequency Cables," *Trans. AIEE*, vol. 68, no. 1, pp. 283-288, July 1949.

E.W. Kimbark, *Electrical Transmission of Power and Signals*, Wiley, 1949.

J.D. Ryder, *Networks, Lines, and Fields*, Prentice-Hall, 1949.

S. Ramo and J.R. Whinnery, *Fields and Waves in Modern Radio*, Wiley, 1949.

W. Jackson, *High Frequency Transmission Lines*, Methuen, 1945.

R. King, "Transmission-Line Theory and Its Applications," *J. Applied Physics*, vol. 14, no. 11, pp. 577-600, Nov. 1943; errata, vol. 15, no. 3, p. 292, Mar. 1944.

R.I. Sarbacher and W.A. Edson, *Hyper and Ultrahigh Frequency Engineering*, Wiley, 1943, Chapter 9.

J.C. Slater, *Microwave Transmission*, McGraw-Hill, 1942.

R. King, "General Amplitude Relations for Transmission Lines with Unrestricted Line Parameters, Terminal Impedances, and Driving Point," *Proc. IRE*, vol. 29, no. 12, pp. 640-648, Dec. 1941.

F.E. Terman, *Radio Engineering*, McGraw-Hill, 1937.

E.A. Guillemin, *Communication Networks, Vol. II: The Classical Theory of Long Lines, Filters and Related Networks*, Wiley, 1935.

W.L. Everitt, *Communication Engineering*, McGraw-Hill, 1932.

C.P. Steinmetz, *Elementary Lectures on Electric Discharges, Waves and Impulses, and Other Transients*, McGraw-Hill, 1914.

H.B. Dwight, *Transmission Line Formulas for Electrical Engineers and Engineering Students*, Constable, 1913.

A.E. Kennelly, *The Application of Hyperbolic Functions to Electrical Engineering Problems*, McGraw-Hill and Univ. London Press, 1912.

J.A. Fleming, *The Propagation of Electrical Currents in Telephone and Telegraph Conductors*, Constable, 1911.

W.E. Miller, "Hyperbolic Functions and Their Application to Transmission Line Problems," 4-part article, *General Electric Review*, April – July, 1910.

O. Heaviside, *Electromagnetic Theory*, London, 1893-1912.

O. Heaviside, *Electrical Papers*, London, 1872-1892.

Bob DePierre, K8KI

2207 Covemont Drive, Huntsville, AL 35801; **k8ki@comcast.net**

Extend the Matching Range of Your 80 m Antenna

An inexpensive, easy and accurate way of broad-banding an antenna.

I prefer to use resonant antennas, but 80 m presents special problems. It's an extremely wide band, and it is very difficult to build a reasonable antenna with SWR better than 2:1 across its entire range. My antenna is resonant near the low end of the band (see **Figure 1**). I need to stretch its operating area up to the 75 m area for the few phone contests I like to run every year. For these few contest opportunities I just can't justify purchasing an expensive high power antenna tuner.

However, today's tools allow us to build our own tuners, designed for our own situation, and do it in an elegant manner.

Tools Required for the Job

You will need two important tools to design your own antenna matching unit.

1) A modern antenna analyzer capable of saving its output as a Touchstone file (such as the Rig Expert AA series). The output file must contain the real and imaginary impedance values for each frequency measured. If your analyzer (such as an MFJ-259) cannot save a Touchstone file, you can type the file yourself, see **Appendix 1**.

2) The program *SimSmith* by Ed Harriman, AE6TY, is available as a free download from **www.ae6ty.com**. You can learn all about this program in online YouTube videos **[1]**. You really don't need to learn a lot about it to design your tuner.

You start by sweeping your analyzer through the range of the band you want to match, then saving your Touchstone file. Then you tell *SimSmith* to load the file. As shown in **Figure 2**, you can also tell *SimSmith* to generate 2:1 and 3:1 SWR circles. You can see here that only the bottom 100 kHz of the band is inside the 2:1 circle. That's not too good.

The beauty of this solution becomes evident as the program not only allows you to sweep the frequency of the antenna trace, but allows you to build a matching circuit

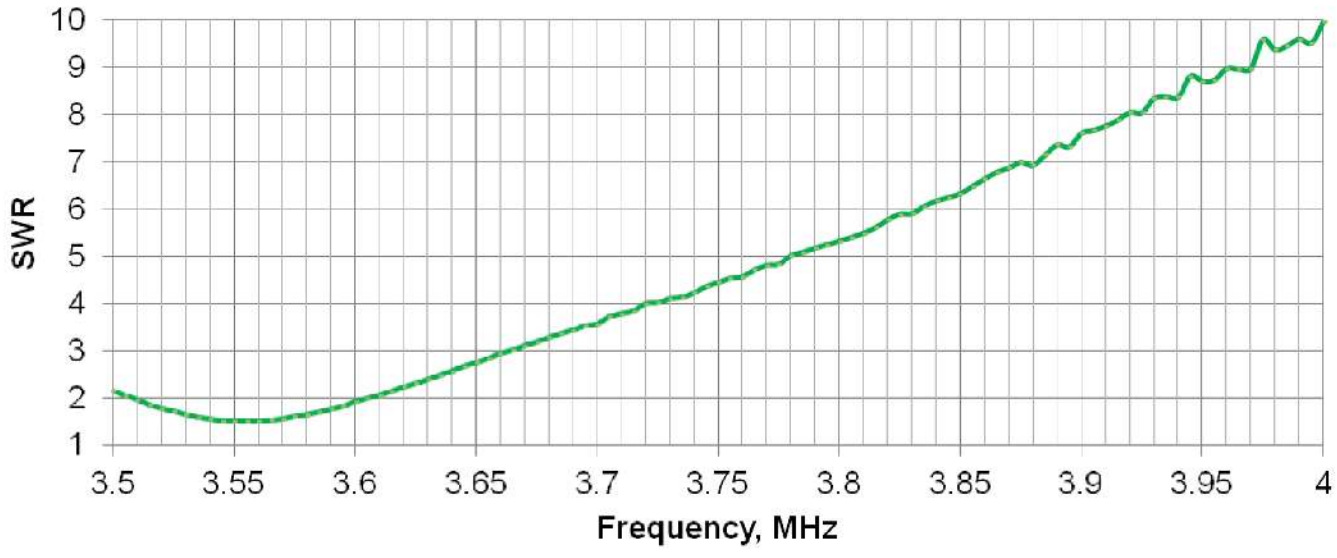

Figure 1 — An 80 m antenna resonant at low end of the band.

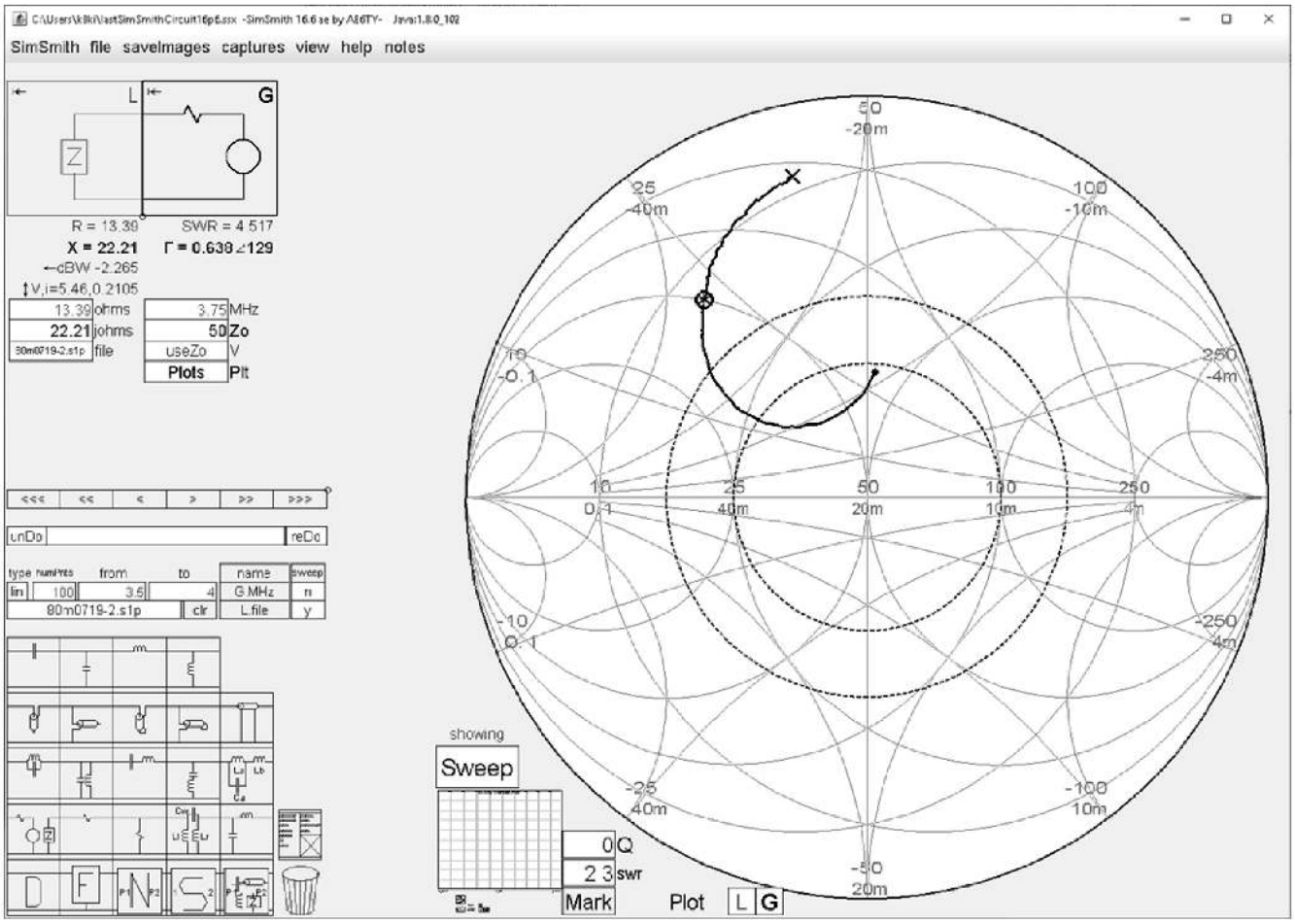

Figure 2 — Impedance trace for 80 m antenna using *SimSmith*.

whose values you can also sweep with a mouse.

You can see a capacitor tuner in the simulated circuit at the upper left corner of **Figure 3**. **Figure 4** shows the result of adding simply a shunt capacitor, connected in the antenna line at the back of your rig. In the Figure 3 Smith Chart graphic, you can see the original antenna trace, as well as the rotated rendition of it as the capacitor is tuned. Here the capacitor is set to 961 pF, optimal to this situation. We now have a circuit that stays inside the 2:1 SWR circle from 3500 to 3825 kHz, and it is done with one capacitor with a couple of connectors and a box (**Figure 5**).

The Concept of Good Enough

Luckily, this problem was solved with just a single inexpensive component. Other situations may also involve a second component, either capacitive or inductive, but those components are almost always going to be small and easy to find or build. More importantly, the aim was not to find the perfect 1:1 solution, but rather to find one that is more universal. That is, one that maximizes the frequency span where the SWR is workable. Very many rigs today have built-in tuners that can easily handle a 2:1 SWR, but maybe not 3:1. If that is your case, your rig can now tune the major part of the 80 m band, which is good enough.

Well, Did It Work?

The trace of Figure 4 shows the circuit response after the capacitor was inserted. It is virtually identical to the simulation of Figure 3. The solution will indeed work, but two other issues must be taken into account to work in the real world.

1) The capacitor must be able to withstand the voltage impressed upon it by the transmitter, as well as the high SWR on your transmission line. See **Appendix 2** for the calculation of the required breakdown voltage.

2) The capacitor must be temperature-stable under the worst conditions. Do not use capacitors with X7R temperature profiles. You must use NP0 capacitors. Perfect capacitors do not dissipate any heat, but our real-world capacitors have an Equivalent Series Resistance (ESR) that does cause them to heat up. Get capacitors with the lowest ESR you can find.

In a first experiment I used a 2 kV, 1000 pF, X7R capacitor with significant ESR. At 660 W, its temperature rose 40 °F. Of course the match flew off the chart. I replaced it with a 2 kV, 1000 pF, NP0, surface mount capacitor with the lowest ESR I could find. Of course it cost ten times as much as the first capacitor, but at 900 W, the temperature rose only 10 °F, and the match didn't budge. Pass! The finished project is shown at Figure 5.

Conclusions

1) Modern antenna analyzers and software offer solutions we couldn't dream of just a short time ago. Use them.

2) Don't try for perfect, single point solutions. "Good enough" swept solutions are far more universal and useful.

3) Use components made for the job. If the job is temperature critical (it always is), use NP0 capacitors with the lowest ESR you

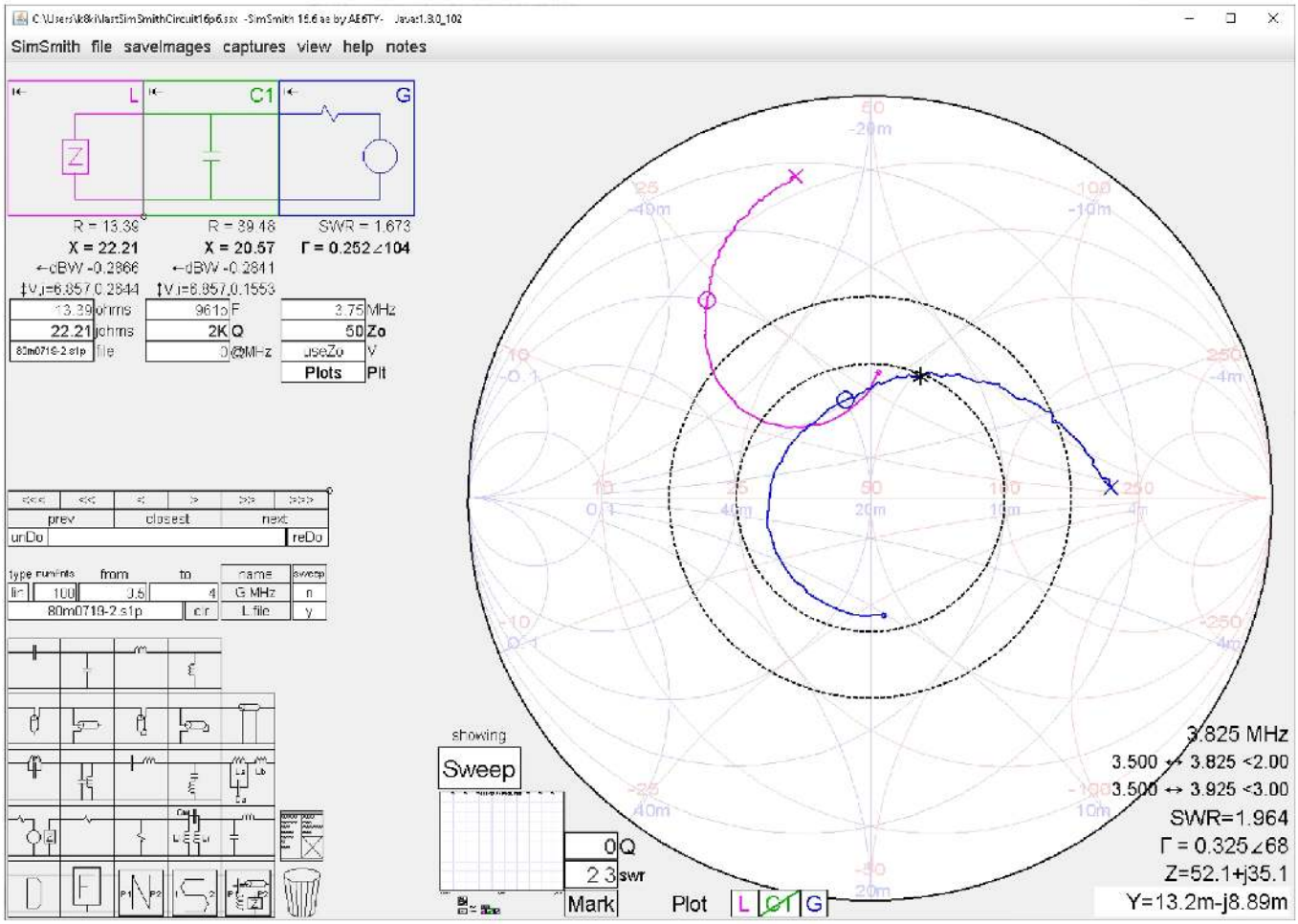

Figure 3 — Sweeping a matching circuit.

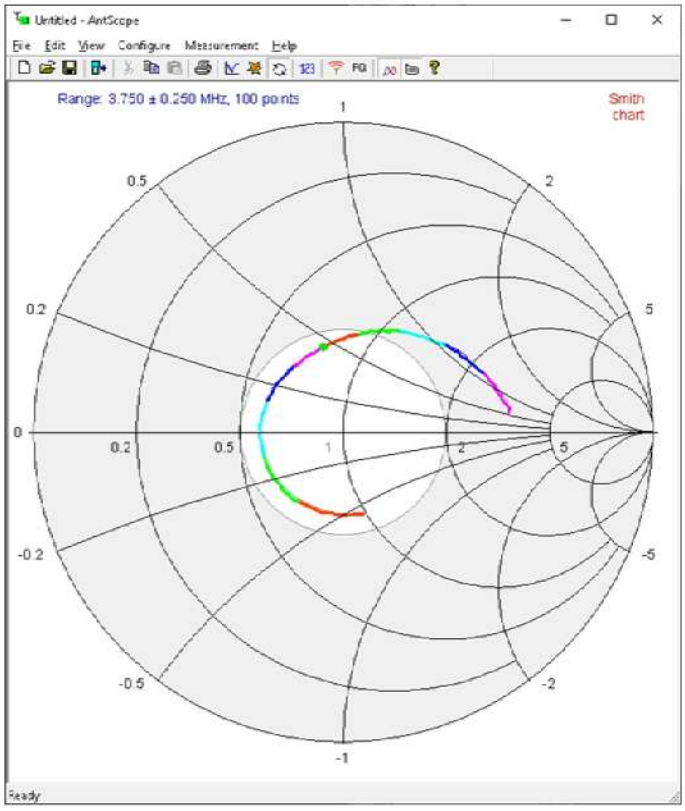

Figure 4 — Antenna sweep with tuner Installed.

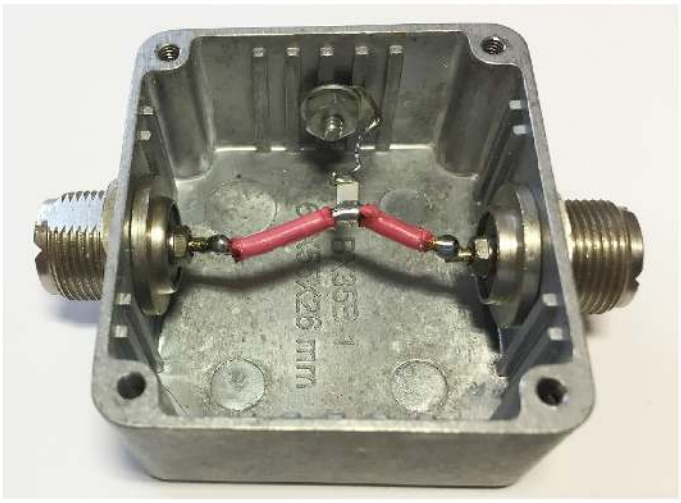

Figure 5 — This 80 m tuner uses a single capacitor.

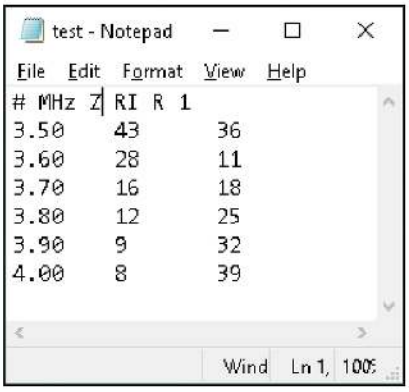

Figure 6 — Touchstone file entered every 100 kHz.

can find. Of course you need ample voltage breakdown headroom as well.

Appendix 1 — Construct Your Own Touchstone File

You can make your own Touchstone file if you have an analyzer such as a MFJ-259, as shown in **Figure 6**. You just open the Windows *Notepad* text processor and enter the first line exactly as shown. It is important that the last number in the first line is a 1, to show the values are normalized to 1 Ω Here I used the *R* and *X* values from my analyzer, except they were spaced every 100 kHz. The fields are: frequency in MHz, the real component of the impedance, and then the imaginary part. Use the Tab key to separate the fields on each line, and a Return at the end of the line. Finally, save the file to something like *test.s1p*. Be sure to use the file suffix *s1p*, and not *txt*.

As you can see in **Figure 7**, the curve is not nearly as smooth as in Figure 3, but your tuning result will be very close. In this case the solution was a 1000 pF capacitor for both 101 points and 6 points of data.

Appendix 2 — Calculation of Voltage Across the Capacitor

An amplifier at 1500 W working into a 50 Ω load will generate:

$$V_{RMS} = \sqrt{PR} = \sqrt{1500 \times 50} = 274$$

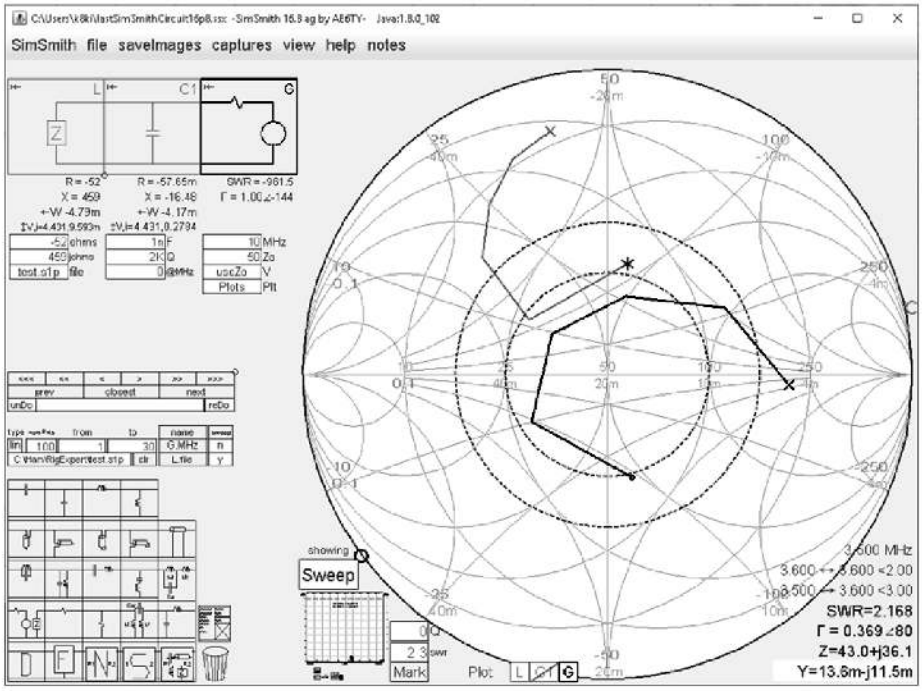

Figure 7 — *SimSmith* solution every 100 kHz instead of every 5 kHz.

The total voltage across a shunt capacitor is:

$$2\sqrt{2} \times 274 \text{ V}_{RMS} = 774 \text{ V}_{\text{P-P}}.$$

The peak transmission line voltage is much higher than this with a high SWR on the line. We can calculate the impact from:

$$SWR = \frac{|V_{max}|}{|V_{min}|} = \frac{1+|\Gamma|}{1-|\Gamma|}.$$

Now for SWR=10, we solve for $|\Gamma| = 9/11$, so that

$$V_{max} = (1+|\Gamma|) \times 774 \text{ V}_{\text{P-P}}$$
$$= (1+9/11) \times 774 = 1408 \text{ V}_{\text{P-P}}.$$

Thus a 2 kV-rated capacitor would give acceptable margin. NP0 and low ESR capacitors are readily available from distributors. Surprisingly, surface mount capacitors as small as size 1812 will meet the specification. Of course larger ones will work as well.

Bob DePierre, K8KI, spent a career in the USAF, and the last 16 years as VP Engineering at the Q-Track Corp. He earned a BSEE at Notre Dame and MSEE at the University of Florida. He is currently president of the North Alabama DX Club. Now mostly retired, Bob enjoys spending time with his new granddaughter, Diana. He has been licensed since 1962.

Notes

[1] See for example **https://www.youtube.com/watch?v=Xf_S2IT4_JE&t=5s**

Jacek Pawlowski, SP3L

Drzonków – Krucza 6, 66-004 Zielona Góra, Poland; **sp3l@wp.pl**

Collection of Broadband HF Antenna Designs, Part - 2

Additional new broadband wire antennas result from an application of optimization software to antenna numerical analysis software.

[This article is presented in three parts. This Part – 2 contains Sections 8 through 10 with antenna detail Figures. Part – 3 is the online **QEXfiles** component that was uploaded for Part 1, Mar./Apr. 2020 *QEX*. It contains all of the Figures, including Figures that show antenna performance details. The Figures of Parts – 1, 2, and 3 are sequentially numbered. — *Ed.*]

8 – Multi-Loop Antennas

I called this class of broadband antennas "Multi-Loop" because their wires are so arranged that you can find many wire loops through which current can flow from one terminal to the other terminal of the antenna feed point. Let's start with probably the simplest Multi-Loop, I call it the Origami-01.

8.1 – Origami-01

The feed point of this antenna is located right in the center of a 7.2 m wide and 4 m high rectangle loop. There are six wires connecting both ends of the feed point with the corners of the rectangle and the centers of rectangle vertical sides as shown in **Figure 33**.

The antenna feed-point impedance is close to 300 Ω and a 6:1 current balun is required for 50 Ω coax. Although a 6:1 current balun is a bit more complex than a 4:1 Guanella balun, it is still easily constructed. However, you may choose to use a 4:1 Guanella balun and 75 Ω coax. This will not create a problem if your transceiver has a built-in Antenna Tuning

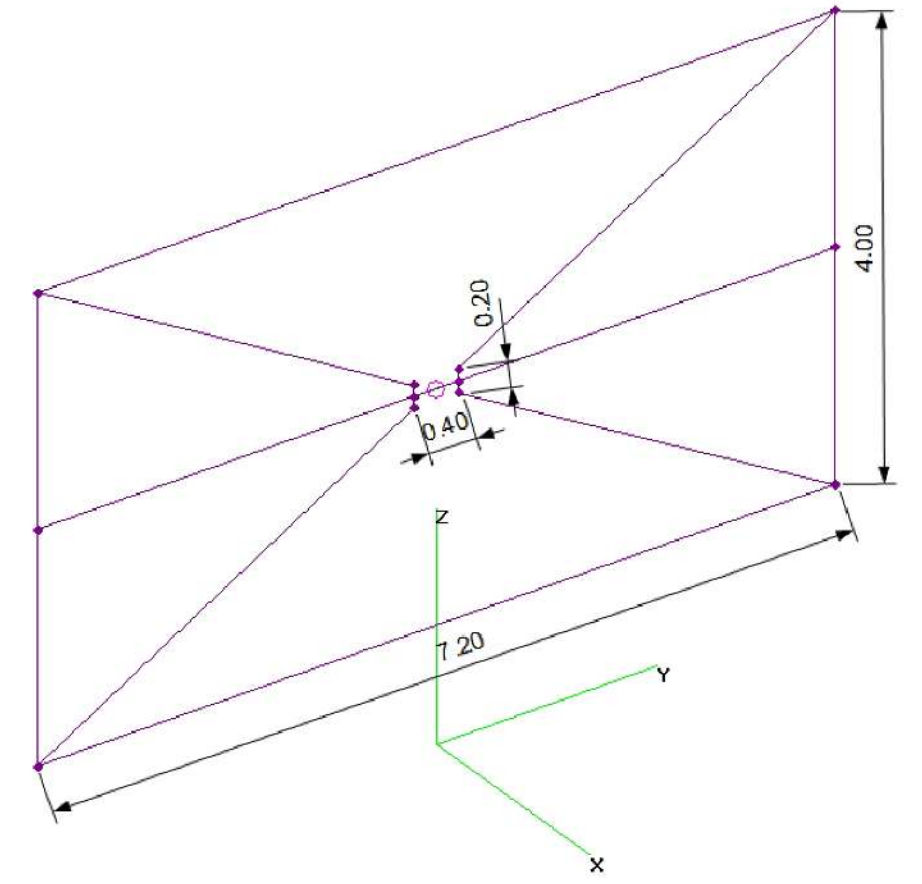

Figure 33 — A view of the Origami-01 antenna.

Unit (ATU) or you have an external antenna tuner connected between the transceiver and 75 Ω coax.

The turning radius of Origami-01 (3.6 m) is smaller than the radii of previously presented antennas, and can be important in some station locations. **Figure 34** (**QEXfiles**) present SWR_{ANT} and gain plots of the Origami-01 and **Figure 35** (**QEXfiles**) shows the radiation patterns for three frequencies. The relative gain of Origami-01 is -0.4 dBdm at 14 MHz and +1.1 dBdm at 29.7 MHz. A 'dBdm' [that is, a modified dBd that includes extra losses due to SWR, where the usual 0 dBd = 2.15 dBi — *Ed.*] unit will be used throughout this paper.

8.2 – Origami-02

This antenna has more wires coming out from the feed point — not six but eight. In this Origami version, those wires are connected to the vertical sides of the outer rectangle frame at 1/3 and 2/3 of their height. The overall antenna dimensions are 7.5 m by 4 m, see **Figure 36**. The antenna feed-point impedance is close to 300 Ω. Its predicted performance graphs are shown in **Figures 37** and **38** (**QEXfiles**).

Origami-02 has lower SWR_{ANT} than Origami-01, which not only makes it a better antenna for the transceivers without ATUs but also results in slightly better relative gains: -0.3 dBdm at 14 MHz and +1.4 dBdm at 29.7 MHz.

8.3 – Cat Whiskers

This antenna is a cousin of Origami-02. In order to make the antenna more convenient to mount on the mast, its feed point was moved downward. As a result, it is only 0.5 m above the lowest wire of the antenna, see **Figure 39**.

A photo image is shown in **Figure 40**. You can a find detailed description of the Cat Whiskers antenna in the March 2018 issue of *QST* magazine.

Figures 41 (**QEXfiles**) presents SWR_{ANT}, and **Figure 42** (**QEXfiles**) shows the gain and radiation pattern plots of the antenna. Its feed-point impedance is close to 300 Ω and its relative gain is -0.2 dBdm at 14 MHz and +1.9 dBdm at 29.7 MHz. The real-world performance of the Cat Whiskers antenna was close to that predicted by the simulation. See the measured SWR_{TRX} in **Figure 43** (**QEXfiles**).

8.4 – Multi-Loop Doublet

The Multi-Loop Doublet is a broadband antenna with a small turning radius. This is very desirable when, for example, your antenna mast is positioned close to a tree or other obstacle. A view is shown in **Figure 44**. This compact antenna is only 6.6 m long, 1.2 m deep and 0.6 m high. Despite its apparent complexity, it is easy to build thanks to its small size

Figure 45 shows a photograph of a constructed Multi-Loop Doublet and **Figure 46** (**QEXfiles**) contains its simulated performance. This antenna performs slightly worse than its bigger broadband cousins. Its gain is -0.9 dBdm at 14 MHz and 0 dBdm at 29.7 MHz. The radiation patterns are quite dipole-like as shown in **Figure 47** (**QEXfiles**).

The first prototype of Multi-Loop Doublet has been operational for more than a year now and its performance is fully confirmed. See the plot of its SWR_{TRX} in **Figure 48** (**QEXfiles**).

9 – Broadband Verticals

Generally, we have two classes of vertical antennas: those requiring connection to the ground radials — like a λ/4 monopole — and the ground independent ones — like the vertical dipole and GP antenna. Let's start with the first class. Such antennas are supposed to have a number of radials buried in the ground or lying on the ground. If your simulator uses the *NEC*-4 engine – no problem. Your simulation results should be accurate then. If, however, you use *NEC*-2 or *MININEC*, you can not be quite sure how much you can trust your results, because those versions of *NEC* do not handle buried radials or radials connected to real ground correctly. There are reports — applicable to the narrow-band resonant antennas — stating that you can simulate buried radials with radials placed slightly above the

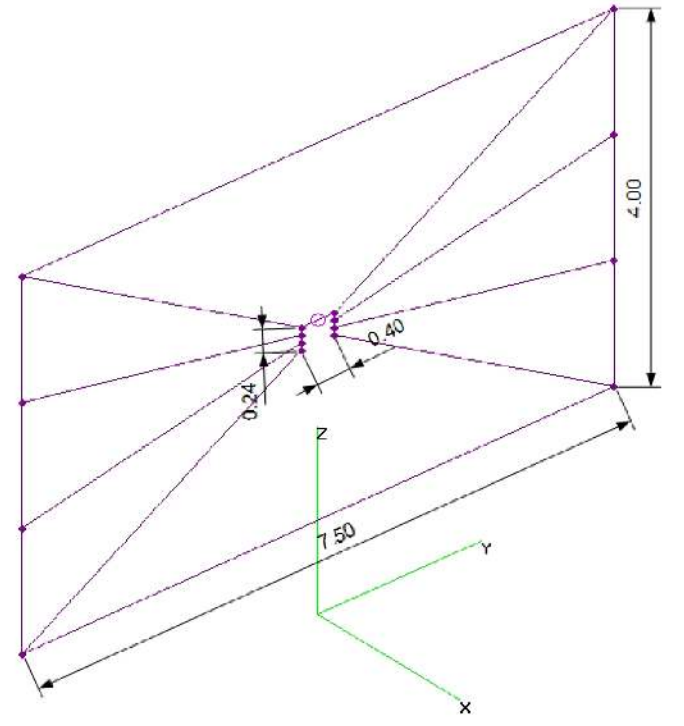

Figure 36 — A view of the Origami-02 antenna.

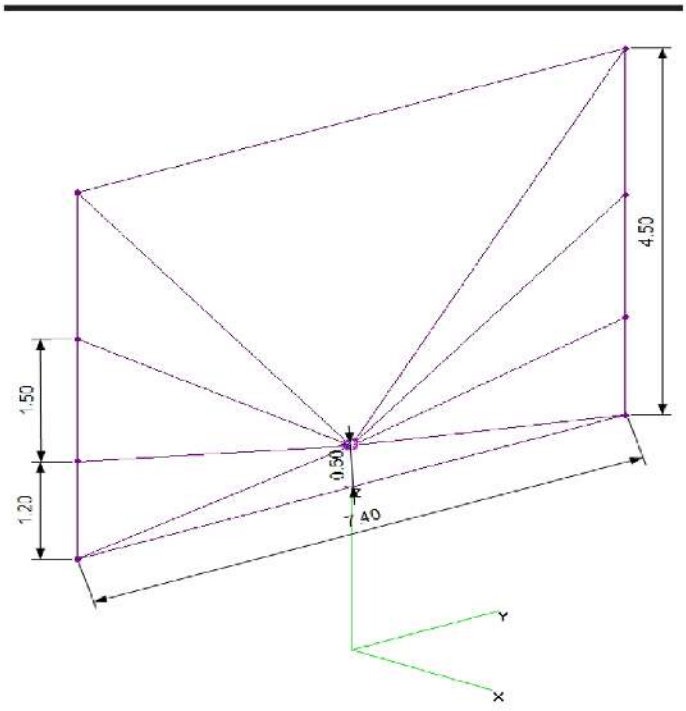

Figure 39 — A view of the Cat Whiskers antenna.

ground. I used this approach but whether it can be applied to broadband antennas is not proven. The results that follow were obtained with *NEC*-2 based simulators. It is very advisable to repeat the simulations with an *NEC*-4 based simulator. Alternatively, one can just construct one of the proposed vertical antennas and measure it. If the *SWR* results are close to the predicted ones, then also the gain and radiation patterns predictions might be trusted as well.

The λ/4 monopole will be a reference antenna to which we will compare broadband vertical antennas in the same way we did with a half-wave dipole and broadband doublets and multi-loops. The reference λ/4 monopole designed for 14 MHz band has a 5.2 m long radiator and 16 same-length radials located 0.01 m above the average ground. Its maximum gain is -0.12 dBi at a pattern elevation angle of 26° see **Figure 49** (**QEXfiles**).

9.1 – Two-element Broadside Monopole Array

One of the simplest ideas for a vertical is to take half of a symmetrical horizontal antenna turn it up by 90° and add a signal source (feed point) at the bottom. Of course, the other terminal of the feed point is grounded. A number and length of radials must be determined during modeling and simulation.

If we take the 2-element BDA and convert it to vertical as explained above, we will create a 2-element BMA. Such antenna is shown in **Figure 50**. The wire containing the feed point is 0.36 m long so the total antenna height is 6.09 m. Every radial is 3.5 m long and is elevated 0.01 m above the ground. The maximum SWR_{ANT} of 3.8:1 occurs at 14 MHz. **Figure 51** (**QEXfiles**) presents SWR_{ANT} and gain plots of the 2-element BMA. If we correct the antenna gain by signal loss due to SWR and compare it with the reference λ/4monopole, we will get -1.6 dB at 14 MHz and +0.6 dB at 29.7 MHz.

The maximum gain occurs at pattern elevation angles of 25°, 21°, 17° for 14, 21.25, 28.5 MHz respectively. The azimuthal radiation pattern is almost an ideal circle at 14 MHz and is slightly deformed to an oval shape at 29.7 MHz, see **Figure 52** (**QEXfiles**). The difference between broadside gain and narrow-side gain is only 0.65 dB — not bad for such a simple antenna.

9.2 – Converging Element Monopoles

The Converging Element Monopole (CEM) is a derivative of the Converging Element Doublet. Three versions were simulated: 3-element CEM, 5-element CEM and 5-element CEM XF with extended frequency range.

9.2.1 – Three-Element CEM

The view of this antenna is shown in **Figure 53**. The antenna is 6.5 m high. It is 20 cm wide at the top and 1.40 m wide at the bottom. There are 16 radials, each 3.50 m long. The 3-element CEM has the highest value of SWR_{ANT} (3.6:1) at 14 MHz and the lowest value (2.1:1) at 26 MHz. If compared to the reference monopole, it

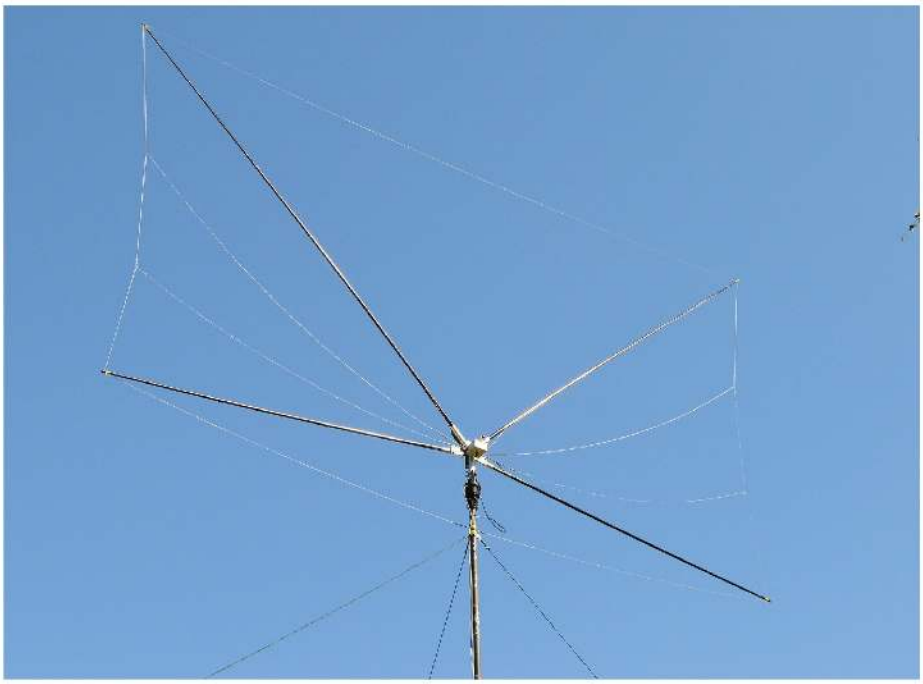

Figure 40 — A prototype of the Cat Whiskers antenna.

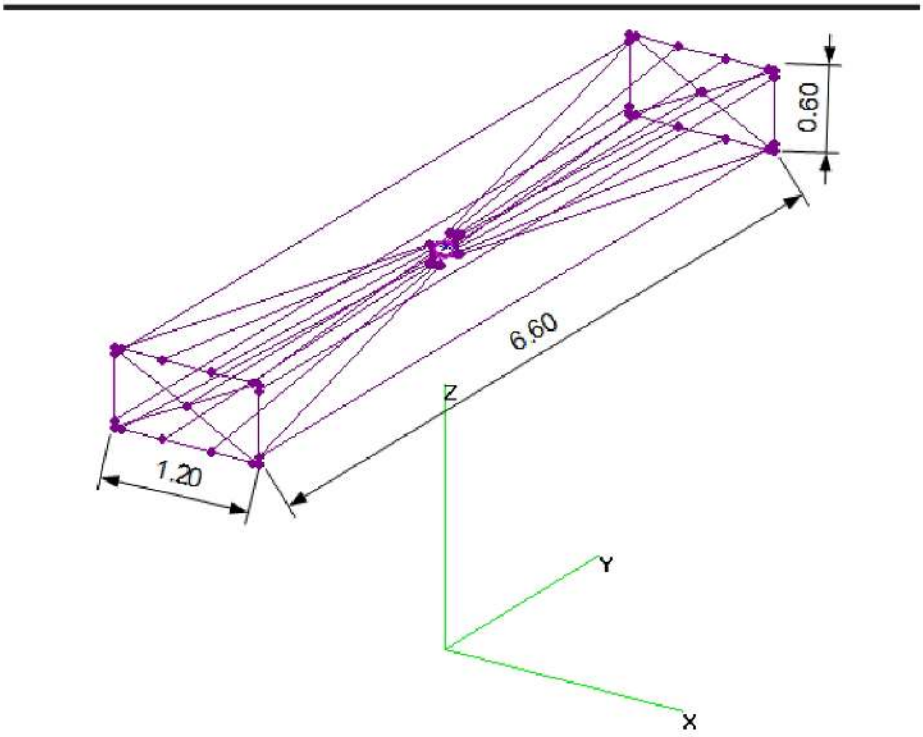

Figure 44 — The Multi-Loop Doublet is a compact antenna.

has relative gain of -1.5 dB at 14 MHz and +0.4 dB at 26 MHz. So, for most of the frequency range, the 3-element CEM produces slightly lower gain than the reference antenna. However, the difference is not big and simplicity of this antenna is striking. It requires a 4:1 un-un matching transformer because its feed-point impedance is approximately 200 Ω.

Its SWR_{ANT} and gain plots are shown in **Figure 54** (**QEXfiles**) and radiation patterns in **Figure 55** (**QEXfiles**). Its azimuthal radiation pattern is practically omnidirectional, the difference between *X* and *Y* axis gain is of the order of just 0.1 dB.

9.2.2 – Five-Element CEM

If we increase the number of converging elements, we can achieve slightly better performance. The 5-element CEM, though a bit more complex, has better SWR_{ANT} and better gain than the 3-element variant. The antenna is shown in **Figure 56**.

The 5-element CEM is shorter — 6 meters instead of 6.5 m — but the remaining dimensions are unchanged. Every outer element is 70 cm away from the central one at the antenna bottom and 10 cm away at the top. The very bottom wire containing the feed point is 60 cm long. The antenna was modeled with 16 radials, each 3.5 m long and 1 cm above the ground. The 5-element CEM requires a 2.25:1 un-un matching transformer because its feed-point impedance is approximately 112 Ω. Such a transformer can be built using one ferrite core, see **Figure 57** (**QEXfiles**).

When compared with the 3-element version, the 5-element CEM has lower SWR_{ANT} and higher gain. You can see in **Figure 58** (**QEXfiles**) how those parameters change over the frequency. The highest SWR_{ANT} is 3.3:1 at 18.5 MHz, and the lowest is 1.1:1 at 28.25 MHz, see **Figure 59** (**QEXfiles**). Compared to the λ/4 reference monopole, it has relative gain of -1.3 dB at 14 MHz and +1.4 dB at 28.25 MHz.

9.2.3 – Five-Element CEM with Extended Frequency Range

If you increase the height of a 5-element CEM by 0.6 m and move the outer elements closer to the central element (reduce the bottom distance from 0.7 m to 0.5 m), your antenna will become even more broadband, and will cover 6 bands from 10.1 MHz to 29.7 MHz. The remaining dimensions are left unchanged, see **Figure 60**. To distinguish it from its basic version, I called this antenna a 5-element CEM XF (eXtended Frequency).

You can see in **Figure 61** (**QEXfiles**) how this antenna radiates at different frequencies. The 5-element CEM XF, see **Figure 62** (**QEXfiles**), has a maximum SWR_{ANT} equal to 3.6:1 at 10.1 MHz and minimum SWR_{ANT} equal to 1.5:1 at about 27 MHz. Note that the SWR_{ANT} was calculated for the source internal resistance 112 Ω. In other words, this antenna requires an un-un with 2.25:1 impedance ratio like the basic 5-element CEM. Its relative gain with respect to the reference λ/4 monopole is -2.1 dB at 10.1 MHz and +1.0 dB at 27 MHz.

9.3 – Manta Ray

If all the verticals covered so far are too tall for you, you may be interested in the Manta Ray. You can see in **Figure 63**, how the antenna got its name. It is totally flat and is only 4.25 m high. **Figure 64** shows the wire connections you need to make near the feed point. The Manta Ray performance plots are shown in **Figure 65** (**QEXfiles**).

Figure 45 — A prototype of the Multi-Loop Doublet.

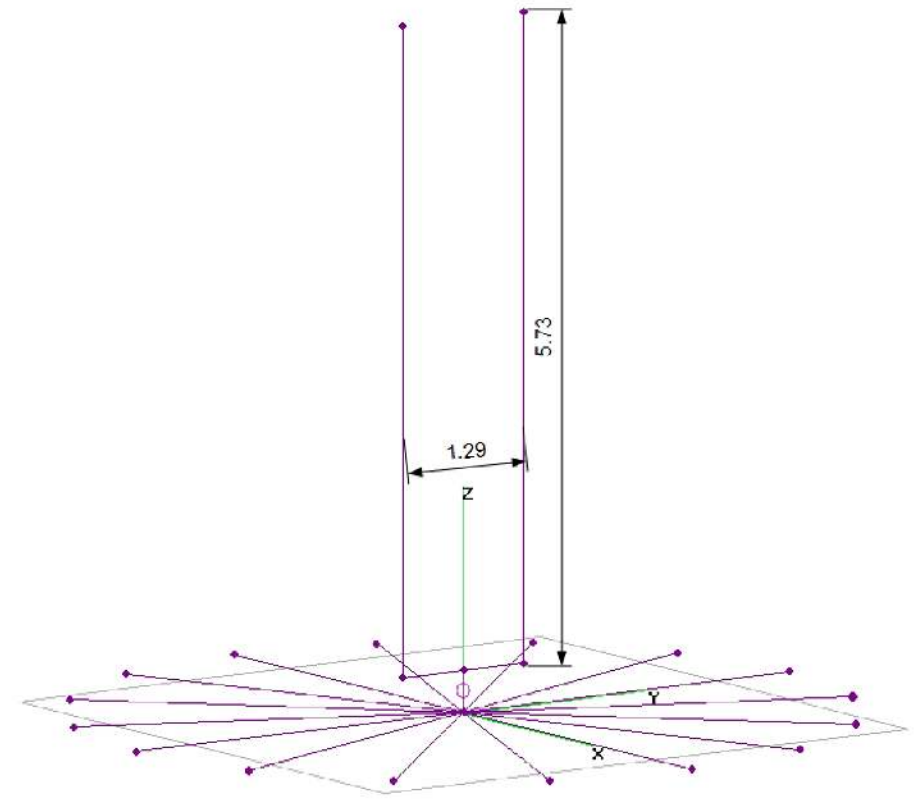

Figure 50 — Two-element BMA main dimensions.

The antenna feed-point impedance is close to 50 Ω so you may feed it directly with 50 Ω coax. It has been modeled with 16 radials 3.5 m long each. Its SWR_{ANT} changes from 1.6:1 at 29 MHz through 3.2:1 at 24 MHz. **Figure 66 (QEXfiles)** presents its radiation patterns. Because of the Manta Ray flatness, the antenna azimuthal radiation pattern is slightly oval, especially at higher frequencies. The antenna gain related to the reference monopole is equal to -1.5 dB at 14 MHz and +1.5 dB at 28 MHz. The Manta Ray has been built and measured. The real antenna had 2 radials, each 3 m long and 2 radials, each 5 m long.

All four radials were lying on the ground, but due to high grass were not very close to it. See the photograph in **Figure 67**. Its SWR_{TRX} is shown in **Figure 68 (QEXfiles)**. Note that it is lower than the simulated SWR_{ANT} because RG-58 is not a lossless transmission line, and 35 m of this cable was between the Manta Ray and antenna analyzer.

Although the real *SWR* profile was not exactly as predicted by the simulator, the antenna really had very wide bandwidth. The 4 radials were enough to ensure a good impedance match — actual SWR_{TRX} below 2:1 for any frequency if measured together with the coax cable — but you should use 16 or more radials to keep ground losses low.

This is a common problem for all the verticals described above — they need a good RF ground, which means many radials. Otherwise the signal will be attenuated due to high losses in the ground. If so, why not design a broadband vertical that uses elevated counterpoises rather than radials?

9.4 – Five-Element CEM GP

Before analyzing this antenna, we need again a reference to which we could compare its performance. You will not be surprised that I chose a λ/4 GP as the reference antenna. Its gain in free space is equal to 1.58 dBi.

The 5-element CEM GP is a modification of the 5-element CEM. The 16 radials are replaced with 4 counterpoises, each 4 meter long, each creating a ground plane for the antenna. **Figure 69** shows the antenna dimensions. The antenna feed-point impedance is close to 112 Ω, so it needs a 2.25:1 un-un transformer.

The antenna SWR_{ANT} minimum is 1.4:1 at 28.25 MHz and maximum is 3.9:1 at 14 MHz. If compared to the reference λ/4 GP antenna, the 5-element CEM GP has relative gain -1.0 dB at 14 MHz, +0.6 dB at 28.25 MHz. Its SWR_{ANT} and gain plots are shown in **Figure 70 (QEXfiles)** and radiation patterns in **Figure 71 (QEXfiles)**.

This antenna is asymmetrical with respect to the ground and need not be installed close to ground. Therefore, except for the impedance matching 2.25:1 un-un transformer, it requires RF common-mode chokes. Simulations showed that if two RF chokes are used they would reduce the common-mode current to a negligible level for any length of the coax. Every choke should have the resistive component of its common-mode impedance equal to or greater than 1.5 kΩ for any frequency in the 14 to 29.7 MHz range. One of the chokes should be placed next to the un-un transformer and the other one after a 5 m run of the coax.

You can find a lot of information about the RF chokes in an excellent work of Ian White, GM3SEK, **www.ifwtech.co.uk/g3sek/in-prac/inpr1005_ext_v2.pdf**. Two "high-band" chokes described in his paper are perfect for the 5-element CEM GP.

9.5 – Five-Element CEM GP Mk.2

If 4 m long counterpoise wires are too long for you, there is a way to make them shorter. **Figure 72** shows a modified version Mark 2 (Mk.2) of the antenna where the counterpoise wires are just 2.1 m long. Their ends must be connected with a perimeter wire, and antenna height is increased from 6.20 m to 6.30 m. The rest of antenna dimensions remain unchanged. There is a certain penalty of a small increase of SWR_{ANT}. At 14 MHz, it is now 4.1:1, slightly above the limit set at the beginning of this paper. However due to a significant reduction of counterpoise length, this antenna is still an attractive option.

The 5-element CEM GP Mk.2 performance is almost exactly the same as the basic version with 4 m long counterpoises, see **Figure 73 (QEXfiles)**. The antenna requires a 2.25:1 un-un and two RF chokes to limit the common-mode current as described before for the basic version.

10 – Conclusion

If you have rather limited possibilities to erect HF antennas, a broadband antenna covering several bands can be an excellent solution for you. A broadband antenna is much less sensitive to dimensional accuracy, and makes it easier to construct. Once built and erected, it will not require any trimming – contrary to the multiband resonant antennas. The antennas covered in this collection do not use loading resistors or traps so their gain remains high. Of course, this is not applicable to the very first one – the TFD which was included for reference in Part 1.

The performance of the broadband antennas presented here is quite close to

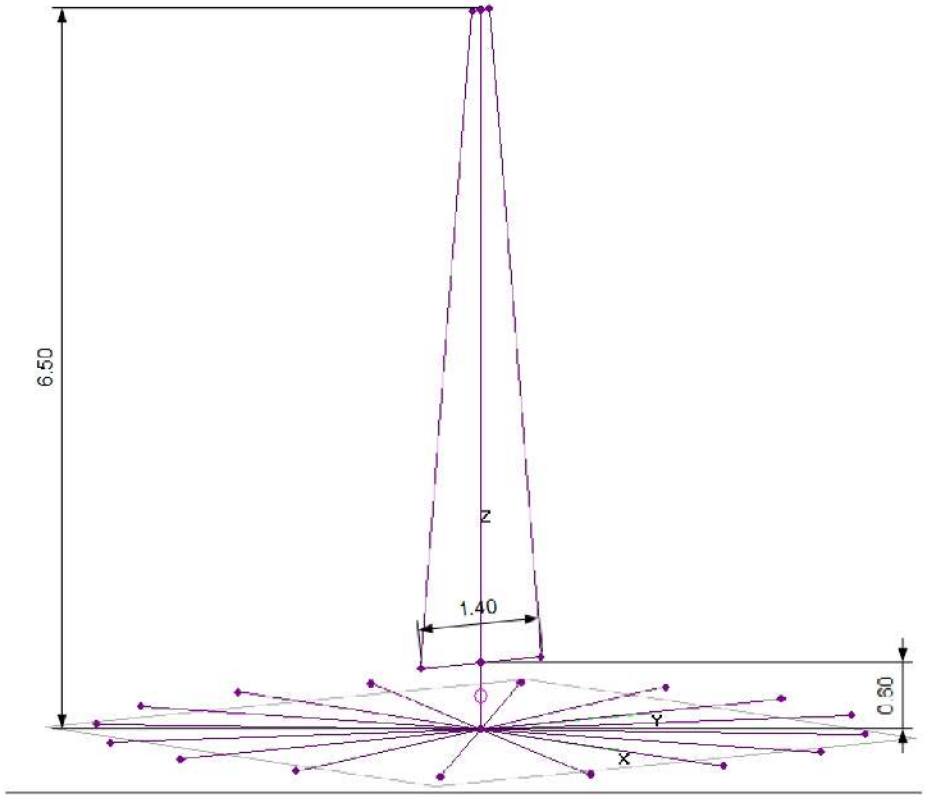

Figure 53 — View of the three-element CEM.

the performance of its monoband resonant counterparts (dipoles or monopoles). Usually, they are slightly worse at the lowest frequency and slightly better at the highest frequency of the operational range.

I built and tested three antennas from this collection. In every case, the antenna worked as expected. So, I am pretty confident that the other designs are also correct and the antennas will work as predicted. The designs were simulated not only with the NEC-2 based simulators (*EZNEC* and 4*nec*2) but also with the *MININEC* based simulator (*MMANA-GAL*).The simulation results were very similar.

I ran an Average Gain Test for every model described here. In all cases, it was quite low (<0.2 dB, sometimes <0.1 dB). This makes me confident that the accuracy of the simulations is good.

Some doubt remains, though, concerning the monopoles requiring RF ground for proper operation. As explained in the beginning of the chapter dedicated to verticals, the actual results can be a little different because radials modeled just above the ground are only an approximation of radials lying on real ground or buried in it. But if you would rather choose ground independent designs (GP versions), the models should be quite accurate. Remember about the RF chokes. GP verticals are by nature quite non-symmetrical with respect to ground. A single RF choke connected near the feed point will not be enough to ensure low common-mode current. Use two of them as explained in the text.

Symmetrical antennas with horizontal polarization described before the verticals, can do without additional RF chokes only if they have Guanella type baluns (current baluns). The common-mode impedance of such a balun should be high. About 3 to 4 kΩ is needed for the antennas having feed-point impedances in the 200 - 300 Ω range. If this is not possible or you are unsure of the value of the common-mode impedance, add an additional RF choke in series with the balun.

The recommended method to keep the common-mode current low for the 450 Ω antenna (like the Multi- Loop Doublet) is to use the 9:1 Guanella type balun and an additional RF choke inserted in the coax 5 m away from the feed point.

If you would like to construct one of the described antennas, a good idea is to take its model, modify it, and run the simulations again. The modification should include wire material and diameter as well as presence of ground. You should model your antenna at the intended installation height. These modifications will significantly influence

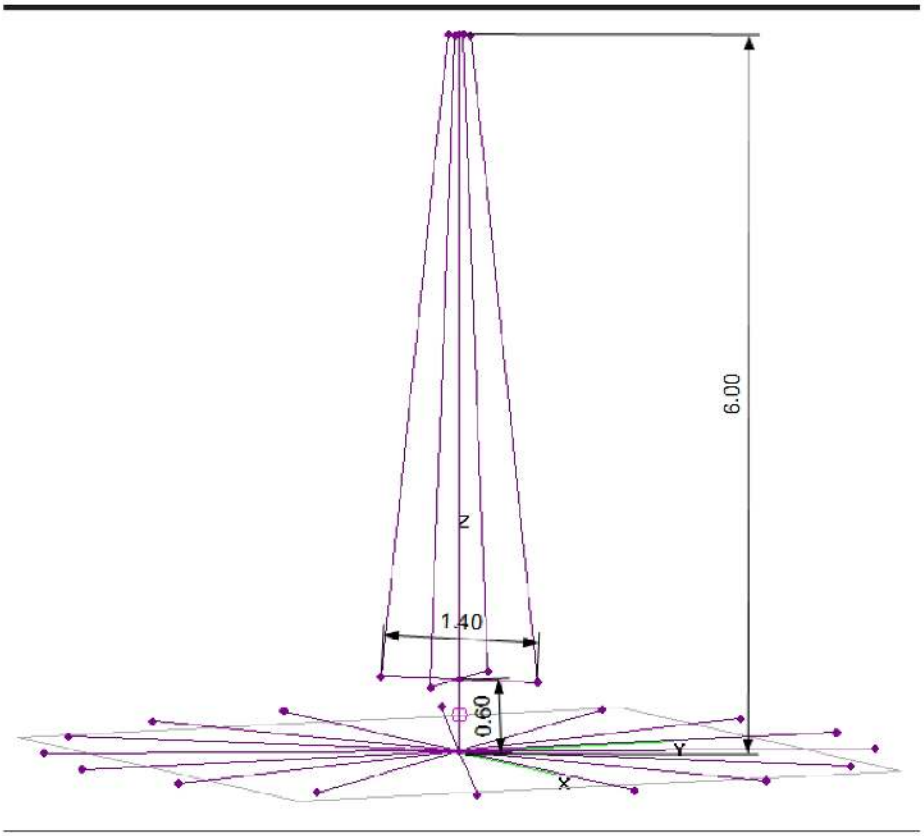

Figure 56 — View of the five-element CEM.

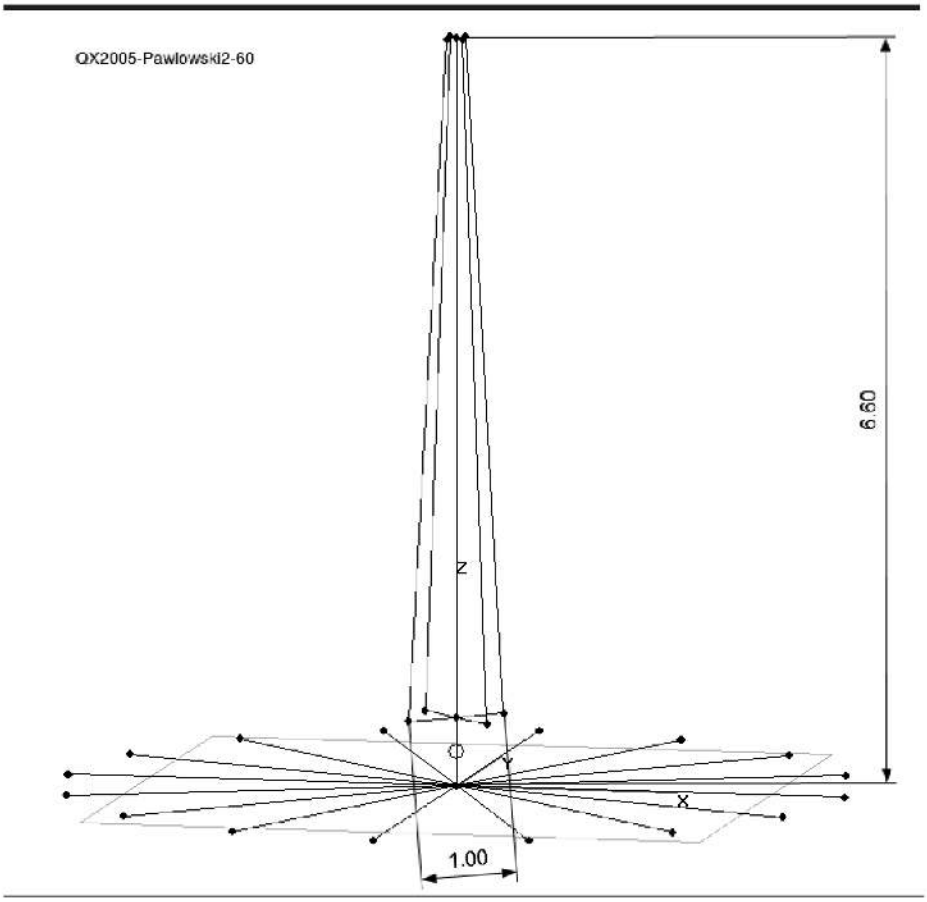

Figure 60 — View of the five-element CEM XF.

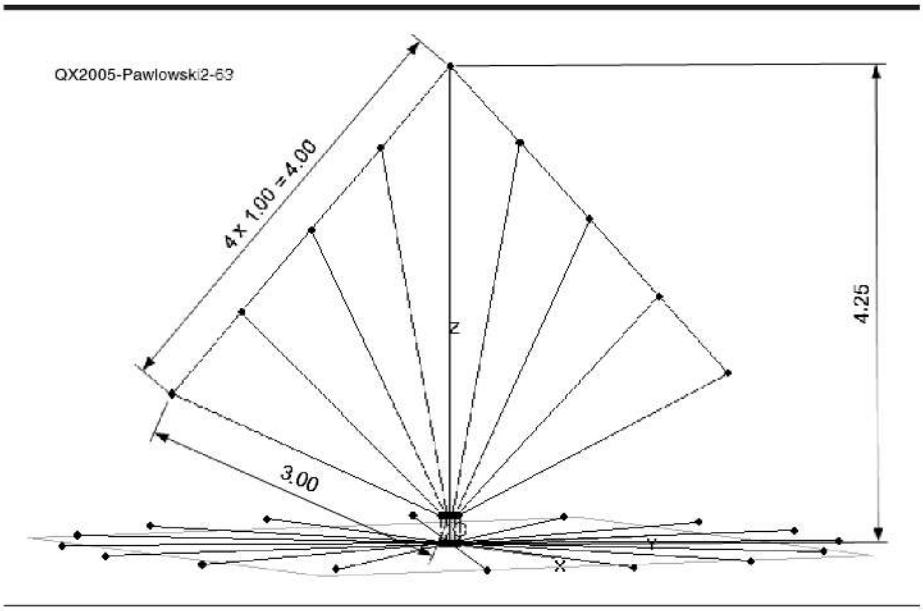

Figure 63 — View and dimensions of Manta Ray.

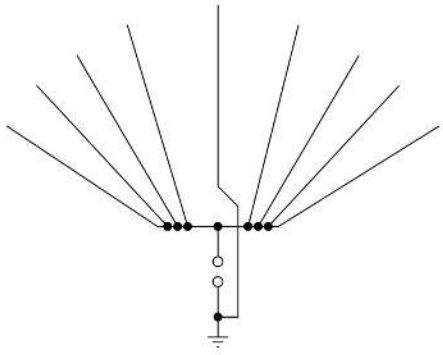

Figure 64 — Wire connections near the feed point of Manta Ray.

Figure 67 — The Manta Ray prototype.

radiation patterns and slightly influence SWR_{ANT}. If you want to get the best possible performance, some adjustment of the dimensions might be needed.

If you are not familiar with antenna simulation programs, you may just construct the antenna with the present dimensions and be ready to accept that the actual antenna SWR can be different over the frequency range. In many cases such differences could be acceptable.

The broadband antenna collection presented here is by no means complete. One can design more antennas with similar features. Naturally, designing a broadband antenna takes more effort than designing a resonant monoband antenna. However, taking into account that a broadband antenna does not require high accuracy in construction, and can work without any trimming after it is installed, the extra time spent on its design pays off.

The biography for Jacek Pawlowski, SP3L, is in Part 1 of this series.

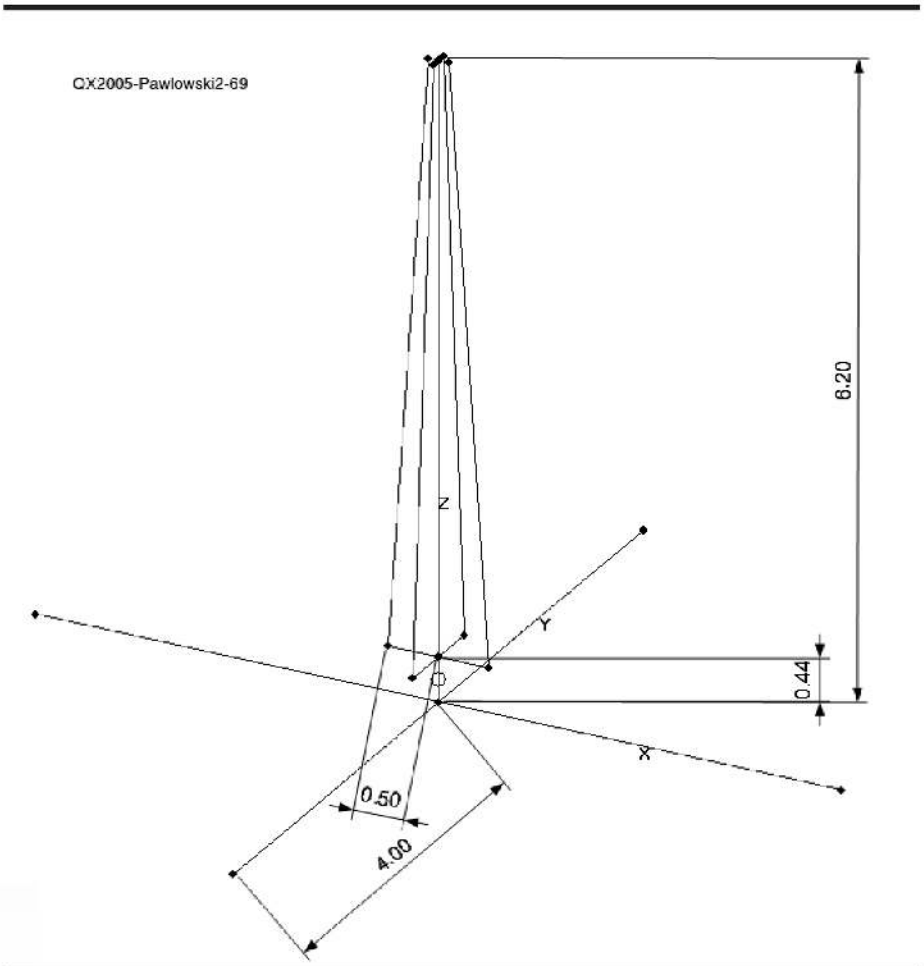

Figure 69 — View of the five-element CEM GP.

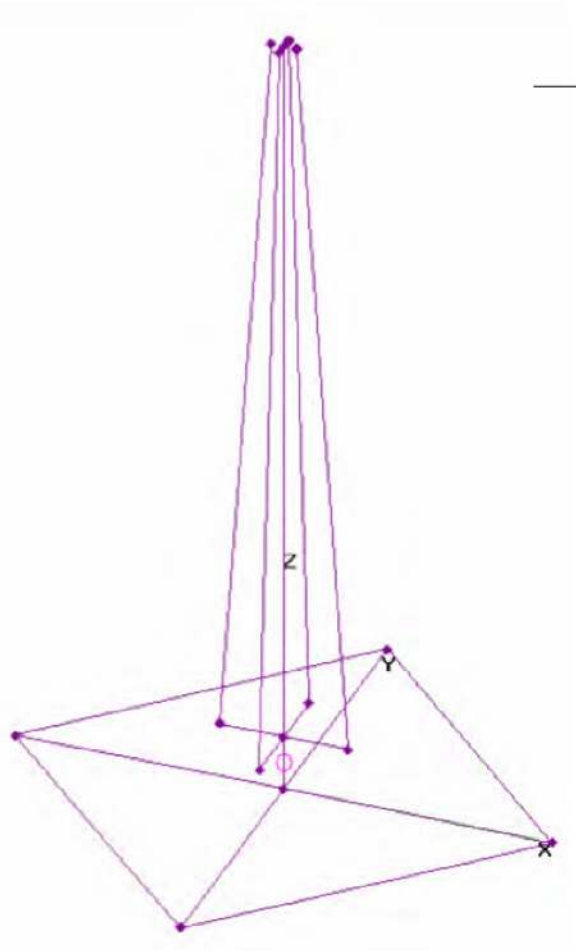

Figure 72 — The view of five-element CEM GP Mk.2.

Upcoming Conferences

Important Alert

Because of the Corona virus pandemic, many organizations are rescheduling or cancelling meetings. Below is the information we have at the time we went to press. You should contact the conference organizer before you book your travel. — Ed.

Central States VHF Society Conference

July 24 – 25, 2020
La Crosse, Wisconsin
2020.csvhfs.org

The 54th annual Central States VHF Society Conference will be held at the Radisson Hotel located on the beautiful riverfront of the Mississippi River in La Crosse, Wisconsin on July 24 – 25, 2020.

This year's event will have all the great activities you've come to expect from a CSVHFS Conference: technical presentations, antenna range, noise figure lab, rover row and dish bowl, Thursday evening social activity, Friday evening trade-fest, dealer room, hospitality suite for evening socializing, fun family activities, and a closing banquet with a guest speaker and a prize table.

Papers are being solicited for publishing in the Proceedings of the 2020 Central States VHF Conference on all weak-signal VHF and above amateur radio topics, including: antennas (modeling, design, arrays, and control); test equipment (homebrew, commercial, and measurement techniques and tips); construction of equipment such as transmitters, receivers, and transverters; operating (contesting, roving, and DXpeditions); RF power amps (single and multi-band vacuum tubes, solid-state, and TWTAs); propagation (ducting, sporadic E, tropospheric, meteor scatter, etc.); preamplifiers (low noise); digital modes such as WSJT, JT65, FT8, JT6M, ISCAT, etc.; regulatory topics; moon bounce (EME); software-defined radio (SDR) and, digital signal processing (DSP).

Topics such as FM, repeaters, packet radio, etc., are generally considered outside of the scope of papers being sought. However, there are always exceptions. If you have any questions about the suitability of a particular topic, please contact Kent Britain, WA5VJB, **wa5vjb@wa5vjb.com**, or Donn Baker, WA2VOI, **wa2voi@mninter.net**.

You do not need to attend the conference nor present your paper to have it published in the Proceedings. Posters will be displayed during the Conference.

Reservations for rooms will open in February. Check website for a hotlink that will take you directly to the Radisson website for event room rate reservations.

The negotiated room rates are available from July 20 through July 28. If you choose to arrive early or extend your stay, these rates will be available to you.

The 39th Annual ARRL and TAPR Digital Communications Conference

www.tapr.org

The 2020 Digital Communications Conference was to be September 11 – 13, 2020 at the Charlotte Airport Hotel, Charlotte, NC. The physical conference has been cancelled. Plans are in the works for a virtual conference. Watch for details.

GNU Radio Conference

www.gnuradio.org

GNU Radio Conference was to be held September 14 – 18, 2020 at the Charlotte Airport Hotel, Charlotte, North Carolina. This conference has been postponed to 2021. Watch for details.

Microwave Update 2020

October 15 – 18, 2020
Sterling, Virginia
www.microwaveupdate.org

Microwave Update 2020, sponsored by the North Texas Microwave Society, will be held at the Holiday Inn, Dulles International Airport, 45425 Holiday Dr., Sterling, Virginia, October 15 – 18, 2020. Information will be added to their website as it becomes available.

Get Ready for Field Day with DX Engineering!

DX ENGINEERING

Field Day Triplexer Combo

Work the 20, 15 and 10 meter bands with three different radios, using just a single tri-band antenna! This package includes Low Band Systems' (LBS) innovative 200W Triplexer, LBS 20/15/10M band-pass filters, and coaxial cable jumpers. Choose from RG8X cable or high-performance RG400. Eliminate the need (and cost) for extra antennas while enjoying fast setup and worry-free operation without RFI. **Enter "Field Triplexer" at DXEngineering.com.**

DXE-200FD-8X-P...$662.93 **DXE-200FD-P...$749.93**

ICOM

IC-7300 HF/50 MHz Transceiver

The IC-7300's RF Direct Sampling System borrows SDR tech to replace the conventional superheterodyne design with an RF Direct system. The result is a versatile and budget-friendly radio that delivers incredible receiver performance, easy filter adjustments and awesome audio clarity.

DX ENGINEERING

Coaxial Cable Assemblies

These low-loss cable assemblies come in standard lengths with DX Engineering's revolutionary patented PL-259 connector. Use the online Custom Cable Builder at DXEngineering.com to build assemblies made to your exact specs. DX Engineering's coaxial cable is also available by the foot or in bulk spools.

DX ENGINEERING

New!

Complete Telescopic Fiberglass Tubing and Cam Lock Clamp Kits

These kits make it easy to set up a reliable temporary antenna mast at home or in the field. They feature durable, smoothly telescoped fiberglass tubing collapsible to either 4 or 7.5 feet for convenient transport. Sections are secured in place with easily adjustable cam lock clamps. Available in heights of 15, 25, and 46 feet. **Enter "Cam Lock Kit" at DXEngineering.com.**

bhi · ICOM · HEIL SOUND · INRAD · KENWOOD · PHONEMA · PRYME · YAESU

Mics, Headsets, Headphones, and Speakers

DX Engineering has everything you need to enjoy clearer audio on Field Day, including lightweight, hands-free headsets; state-of-the-art headphones; noise-cancelling speakers; and premium desktop microphones. We carry leading accessories from bhi, Heil, Icom, INRAD, Kenwood, Phonema, Pryme, Yaesu and others. **Click on "Audio" at DXEngineering.com for our full lineup.**

plasticase NANUK PROFESSIONAL PROTECTIVE CASES · RigExpert®

RigExpert Analyzer and NANUK Case Combos

In the field, an antenna analyzer is especially at risk for weather and shock damage. We've paired select RigExpert Antenna Analyzers with perfectly sized NANUK equipment cases. Each case is filled with cubed, sectioned foam for custom configuration. Also available separately. **Enter "RigExpert Combo" at DXEngineering.com.**

Free Standard Shipping for Orders Over $99*.
If your order, before tax, is over 99 bucks, then you won't spend a dime on shipping. (Additional special handling fees may be incurred for Hazardous Materials, Truck Freight, International Orders, Next Day Air, Oversize Shipments, etc.).

Request Your New Catalog at DXENGINEERING.com!

Showroom Staffing Hours:
9 am to 5 pm ET, Monday-Saturday

Ordering (via phone):
8:30 am to midnight ET, Monday-Friday
9 am to 5 pm ET, Weekends

Phone or e-mail Tech Support: 330-572-3200
8:30 am to 7 pm ET, Monday-Friday
9 am to 5 pm ET, Saturday
All Times Eastern I Country Code: +1
DXEngineering@DXEngineering.com

800-777-0703 | DXEngineering.com

DX 20 YEARS ENGINEERING

CELEBRATING 20 YEARS 2000–20

We're All Elmers Here! Ask us at: Elmer@DXEngineering.com
Email Support 24/7/365 at DXEngineering@DXEngineering.com

YouTube

A PERFECT PAIR

Combine our manually tuned, ultra-portable yet high performance CrankIR Vertical with the SARK-110 pocket sized antenna analyzer!

CrankIR

A lightweight, high performance, extremely portable vertical antenna rated at 1500 watts key-down with fully manual operation (no electrical power or controller required). An optional portable tunable elevated radial system is available and its patented folded design allows for a 40% reduction in size with only 0.3dB reduction in gain performance when compared to a full sized antenna. With available versions that cover 80m-2m and 40m-2m (and every frequency in between), the CrankIR sets up quickly and provides flexibility to change the bands quickly. This antenna is the choice of amateur radio operators and emergency communications teams world-wide, in both portable and permanent applications. Consider purchasing one of our SARK-110 battery powered pocket sized antenna analyzers for use with the CrankIR – a custom 3D printed mounting bracket is available to secure the SARK-110 to your CrankIR!

SARK-110

The SARK-110 antenna analyzer is a pocket-sized instrument that provides fast and accurate measurement of the vector impedance, VSWR, vector reflection coefficient, return loss and R-L-C. Typical applications include checking and tuning antennas (such as the CrankIR), impedance matching, component test, cable fault location, measuring coaxial cable losses and cutting coaxial cables to precise electrical lengths. The SARK-110 has full vector measurement capability and accurately resolves the resistive, capacitive and inductive components of a load. The SARK-110 is intuitive and easy to use, and utilizes four operating modes: sweep mode, smith chart mode, single frequency mode and frequency domain reflectometer (cable test).

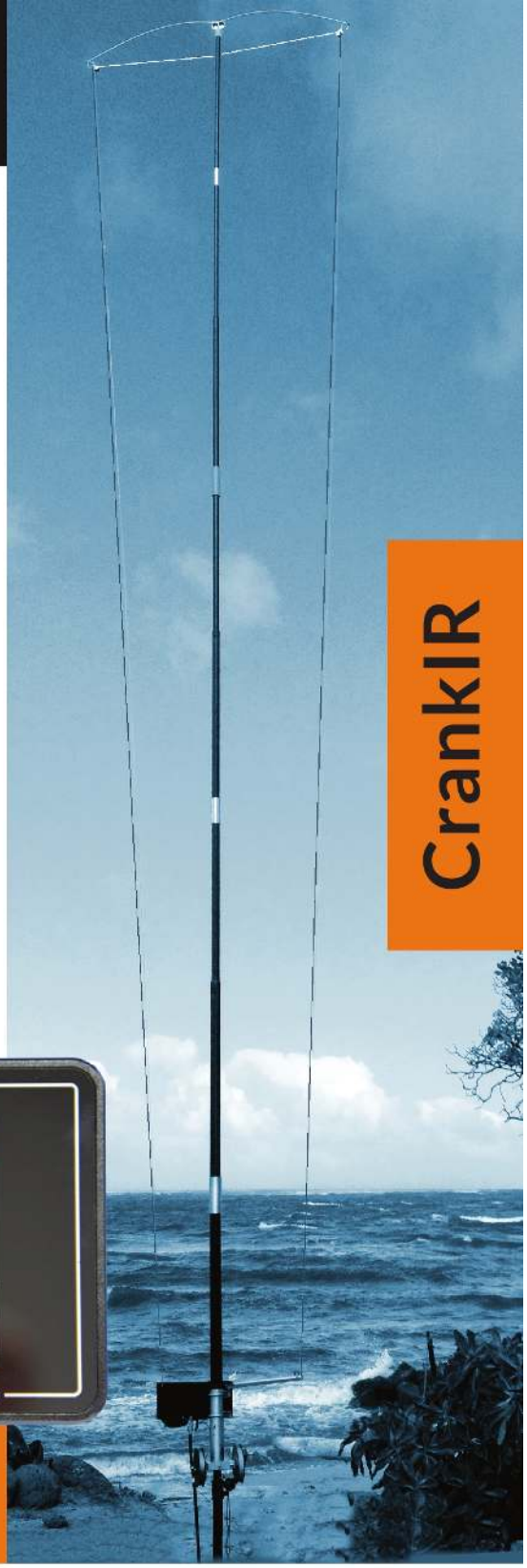

SARK-110

Ask us about our new 3D printed SARK-110 bracket, designed specifically for the CrankIR! *(Prototype holder shown)*

"We introduced the CrankIR to be a world-class portable antenna – little did we know that scores of amateur radio operators would make this their home station antenna as well!"

– John Mertel, WA7IR
CEO SteppIR Communication Systems

steppIR
COMMUNICATION SYSTEMS

FOR DETAILS ON THESE PRODUCTS AND TO ORDER:

www.steppir.com 425-453-1910